



Lucas Caspar Felix Speckbacher, BSc

Implementation of a Single Photon Detector for Satellite Laser Ranging Stations

MASTER'S THESIS

to achieve the university degree of
Diplom-Ingenieur

Master's degree programme: **Electrical Engineering**
submitted to

Graz University of Technology

Supervisor

Ao.Univ.-Prof. Dipl.-Ing. Dr.techn. Erich Leitgeb

Institute of Microwave and Photonic Engineering

Graz, July 2020



This thesis was supported by
Austrian Academy of Sciences

Space Research Institute, department of Satellite Laser Ranging
Group Leader: Dr. Georg Kirchner

AFFIDAVIT

I declare that I have authored this thesis independently, that I have not used other than the declared sources/resources, and that I have explicitly indicated all material that has been quoted either literally or by content from the sources used. The text document uploaded to TUGRAZonline is identical to the present master's thesis.

Graz, July 2020

.....

Acknowledgments

I want to thank everyone who helped me during the process of writing this thesis. Special thanks to Dr. Georg Kirchner and his team at Lustbuehel Observatory who helped in many different ways to make the results possible and offered an insight into the world of Satellite Laser Ranging. Also I want to thank Prof. Dr. Erich Leitgeb as Supervisor who offered a huge freedom and helped whenever questions occurred.

In the end I want to thank my father who supported me throughout my years of study.

Abstract

With a rising number of objects in the orbit of the earth the importance of Satellite Laser Ranging increases, which allows to determine the exact position of the object. One part of this system is the detector which is used to convert the reflected photons into an electrical impulse.

The aim of this thesis is to develop a detector for an SLR system. This prototype has to be tested in the laboratory and the accuracy needs to be identified. For the accuracy measurements in the picosecond range are necessary. Additionally effects that reduce the measurement accuracy will be minimized.

After an evaluation of the boundary conditions the prototype is developed and different types of photo diodes are tested. Additionally a measurement setup is developed where it is possible to change the number of photons and to analyze and save the runtime until detection of the photons. Another part deals with the countermeasures of the photon dependent time walk.

Kurzfassung

Mit der steigenden Anzahl an Objekten im Erdorbits vergrößert sich die Bedeutung von Satellite Laser Ranging, die es ermöglicht, deren Position genau bestimmen zu können. Ein Teil des dazugehörigen Systems ist der Detektor mit dem die reflektierten Photonen in ein elektrisches Signal umgewandelt werden.

Ziel dieser Arbeit ist es, einen Detektor für ein SLR System zu entwickeln, diesen im Labor zu testen und die Genauigkeit zu bestimmen. Für die Genauigkeit sind Messungen im Picosekunden Bereich notwendig. Des Weiteren werden Effekte, die die Messungenauigkeit verringern, stückweise minimiert.

Nach einer Evaluierung der Rahmenbedingungen wird der Prototyp entworfen und verschiedene Photodioden getestet. In weiterer Folge wird ein Messaufbau entwickelt mit dem zum einen die Anzahl der Photonen variiert und die Laufzeit bis zur Detektion der Photonen analysiert und dokumentiert werden kann. Ein Teil behandelt die Gegenmaßnahmen für den Photonen abhängigen Time Walk.

Contents

Abstract.....	v
Kurzfassung	v
1. Introduction to Satellite Laser Ranging	8
1.1 System overview.....	9
1.2 Detector	10
1.3 Laser Requirements.....	11
2. Fundamentals	12
2.1 Photo diode.....	12
2.2 Avalanche photo diode	13
2.3 Single photon avalanche diode	14
2.4 Quenching	15
2.5 Gating	16
2.6 Timing Jitter	16
2.7 Neutral Density Filters.....	17
3. Circuit Implementation	19
3.1 Power supply and cooling	20
3.2 Detector	22
3.3 Using an APD as SPAD.....	24
4. Measurements	27
4.1 Setup	28
4.2 Software	31
4.3 Time measurement.....	32
4.4 Time Walk.....	33
4.5 Measuring at 1064 nm	35
5. Time Walk compensation.....	36
5.1 Concept	38
5.2 Delay Line.....	39

5.3	Measurements	40
6.	Conclusion and Outlook	43
6.1	Conclusion	43
6.2	Future improvements	43
	Bibliography	45
	List of Figures	47
	List of Tables	49
	List of Abbreviations	50
	Appendix	51

1. Introduction to Satellite Laser Ranging

SLR measures the time needed for light to travel from a transmitter to an object and the reflected light back to a receiver. The distance to the objects is nearly half of the measured time multiplied with the speed of light. For a better reflection, satellites can be equipped with specially designed mirrors to direct the light back to the transmitter. These mirrors are called retro reflectors and consist of three perpendicular mirrors that reflect the light right back to the direction of the light source with a big working angle. SLR stations have a resolution in the millimetres range, it is the most accurate method for measuring the position of a satellite. This kind of observation was introduced in 1972 with the start of the first dense spherical satellite LAGEOS-1. To obtain the best results SLR measurement requires a dry correction of the troposphere [1].

The measurements of a network of SLR stations can be combined and a very exact trajectory of satellites can be determined. This knowledge opens a wide field of research. With passive satellites like LAGEOS 1 or 2 geodetic research can be done like measuring the variations in the Earth's gravity field and motions of the stations relative to the geocenter. It enables the study of long term dynamics of the Earth's rotation and orientation as well as changes in the distribution of mass. Furthermore SLR can be used as a reference for altimeter satellites when used in combination with long term climate observation including sea level, ice volume and seasonal variations. SLR also provides a reference for global navigation systems like GPS or Galileo. It can also be used as fall back system when other radiometric tracking systems are failing [2].

To add additional application areas of laser ranging, it can also be used to measure the distance between the earth and the moon by use of reflected photons. This is possible due to retro reflectors put on the moon by Apollo 11, 14 and 15 as well as the two Soviet missions Lunar 17 and 21. These measurements can be found under the term of Lunar Laser Ranging (LLR). The requirements of an LLR station exceed the possibilities of a small or regular SLR station. LLR can be used to describe the lunar emphasis and describe Earth's orientation parameters.

Laser Ranging is one of the strongest tools for testing Einstein's relativistic models and other fundamental physics like the gravitational constant and the mass of the Earth [2] [3].

In recent years, an adopted version of SLR has been used to face the growing amount of space debris. Even satellites without a retro reflector may reflect enough photons from large objects like solar panels or satellite bodies in order to be localized. The biggest change on the system to perform space debris tracking is a changed wavelength from 532 nm to 1064 nm. The advantage of 1064 nm is an increased efficiency, due to lower atmospheric attenuation and no need for a frequency doubling crystal at the laser. The efficiency is increased by approximately 10 times at an elevation of 90 ° and approximately 50 times at an elevation of 20 ° [4].

1.1 System overview

The photons from a laser can be guided to the telescope with mirrors, or a smaller laser can be mounted directly to the telescope. The laser beam itself is a widened collimated beam. To collect as many reflected photons as possible, a telescope is used where the light is focused on the detector. Laser and the telescope have to be pointing to the same direction. As a data source for the estimated satellite trajectory TLE calculated on the base on radar data can be used. TLE is the standard format describing satellite orbits, consisting out of two lines each 69 characters long. The two lines are including a unique satellite number and a checksum, sometimes a third line provides the satellite name for easier handling [6]. The TLE data is acquired by radar and optical observations and can be downloaded from different websites [5].

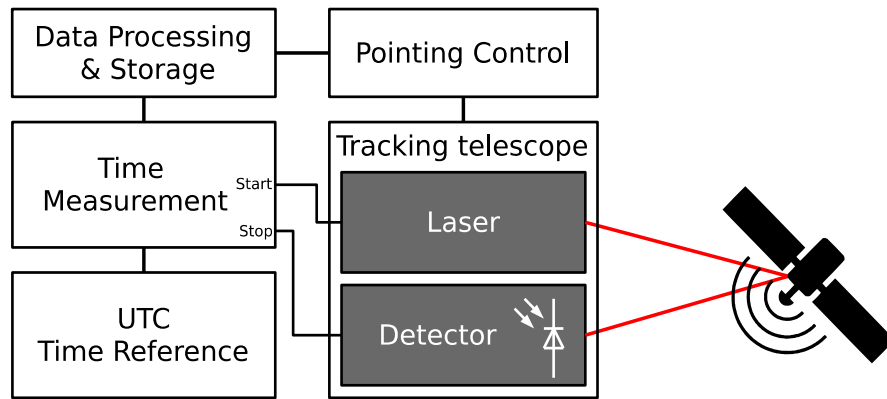


Figure 1: Simple block diagram of a SLR system

The time of flight of the received light pulses has to be measured accurately in the range of 10 picoseconds. The measured pulses are saved with an accurate time reference so that separately measured satellite passes and data from different SLR stations can be combined for analysis.

1.2 Detector

The requirements of the detector are as follows: deterministic output pulses in time domain for a wide range of photons hitting the detector. The number of photons ranges from single photons to 1000 photons per received pulse. The wavelength is limited by a sharp band pass filter. This reduces the detection of background photons to a minimum. Photo diodes have a variation of the detection time, depending on the number of photons. This effect is named time walk. The detector circuit should minimize or extinguish this effect as well as possible.

Beside the background photons internal spontaneous breakdown can trigger an output pulse. To minimize both effects even further, gating is used. In general gating is a correlated measurement and is described in more detail in chapter 2.5.

The task for this thesis is the development of a generic detector for the SLR system at Lustbuehel Observatory based on the given requirements. This includes the development of the schematic, design of the PCB and the testing of the detector. At first a detector for 532 nm is built and then modified for 1064 nm, as the photo diodes for 1064 nm are more expensive than photo diodes for shorter

wavelengths. Parameters like quantum efficiency or dark count rate can primarily be determined by the selection of the photo diode model.

1.3 Laser Requirements

The time resolution of a SLR system is limited to the length of the laser pulse, since it is unknown if the returned photons are originated from the beginning of the laser pulse, the end or somewhere in between. On the other hand, the energy per pulse should be as high as possible, in order to maximize the number of photons emitted in the direction of the target. In the past, longer pulses with a pulse length about 50-100 ps with a high energy about 20-100 mJ per pulse and a low repetition range about 10 Hz were used. At the moment solid state Nd:Van lasers are used with a repetition rate about 2 kHz, an energy of 0.4mJ and a pulse length of 10 ps. Newer lasers with higher repetition rates of 10 kHz and above are tested at the moment [7].

An even higher repetition rate provides challenges to the rest of the SLR system, first of all to the receiver, since the full sensitivity must be restored in a much smaller time than before. For testing in the laboratory another parameter has to be taken into consideration in order to provide consistent test results, the number of photons should stay the same over a longer time period. This attribute is needed to attenuate the pulse manually and test both the dynamic range of the detector and the impact on the time resolution.

2. Fundamentals

An important part of this thesis is the photon detector itself. This chapter describes how detectors work, how they can be used and operated. When working in single photon range, various effects have to be considered.

To detect illumination, two kinds of sensors can be used. Photoconductive cells are composed of junctionless semiconductors. The resistance changes with their illumination, and the basic behaviour is similar to an ohmic resistor. They can be used for low light applications. Disadvantages are a strong temperature dependency and long settling time. The second type uses the reverse current of a diode where the current depends on the illumination. These photo diodes are equipped with a glass window. With an applied reverse current, the photo current keeps the same and the short-circuit current is directly proportional to illumination. This operating mode can be used if short responses are needed, whereas with a higher bias voltage the capacitance of the depletion zone gets smaller. Comparing these two sensor types the photo diode has more advantages for detecting laser pulses [8].

2.1 Photo diode

As described above, the absorption of light in a semiconductor is proportional to the reverse current. There is a high electric field strength in the p-n junction due to the charge carrier-free depletion zone. A free electron would be pushed into the n-zone due to its negative charge, a hole on the other side has a positive charge and would be dragged into the p-zone. An overview of this process in a semiconductor can be seen in Figure 3. Photons can create electron-hole pairs in the depletion zone, by lifting electrons from the valence band into the conduction band. This is called photoelectric effect. The energy of a photon can be described with following equation, where “h” is the Planck constant and “v” is the frequency of the photon. If the energy of a pulse is known the theoretical number of photons can be calculated [9] [8].

$$E = h \cdot \nu$$

Figure 2 shows the energy levels of the valence band at the bottom and the conduction band at the top. In the p-doped area the energy levels are higher than in the n-doped area. The big white arrow shows a photon that generates an electron-hole pair.

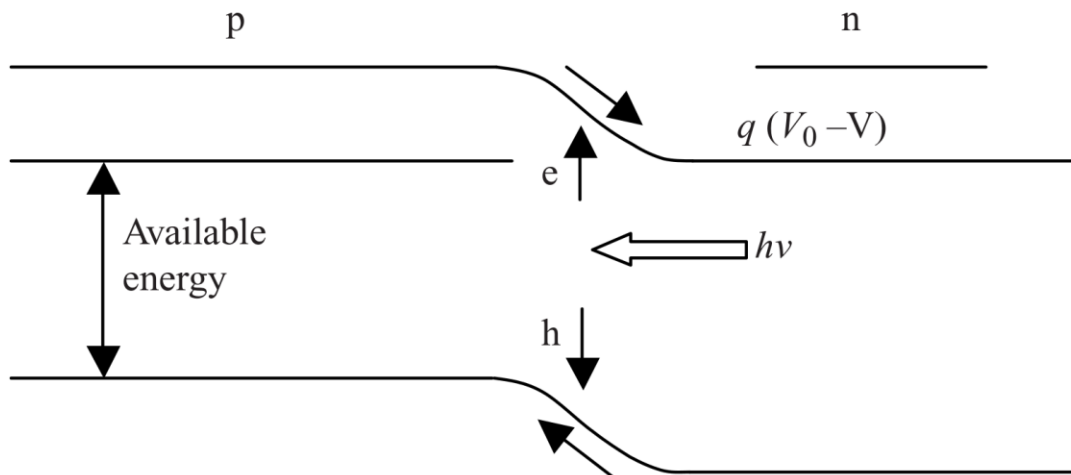


Figure 2: Energy levels in a photo diode [9]

The spectral sensitivity and the energy level of the diode is dependent on the material of the semiconductor.

Silicon based photo diodes have a higher absorption coefficient in the visible spectrum, indium gallium arsenide have higher responsivity in near infrared spectrum. In general, photons with a longer wavelength do not have enough energy to create electron-hole pairs in the semiconductor. The generation of electron-hole pairs is rapidly decaying with depth if the wavelength is shorter [9].

2.2 Avalanche photo diode

Avalanche photo diodes are operated in reverse-biased mode. In comparison with a simpler p-n or pin photo diode, this kind of photo diode uses a high reverse voltage. The higher reverse voltage leads to an avalanche multiplication, which introduces an internal current amplification. The amplification factor depends on temperature and reverse voltage, for APD, 10^2 is a typical amplification factor [10] [11].

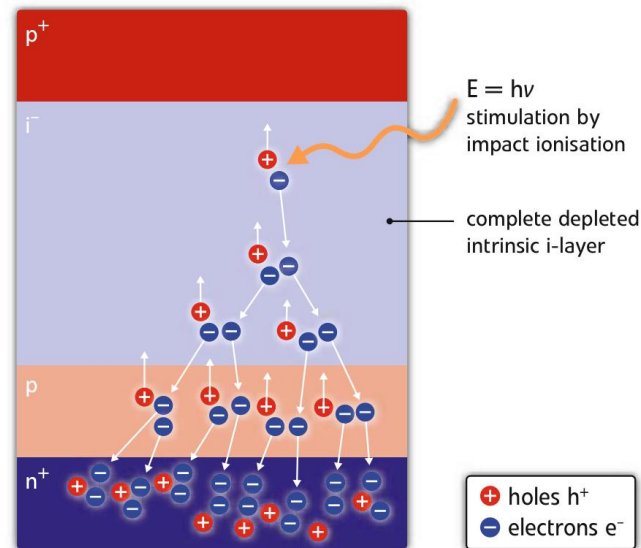


Figure 3: Function principle of an APD [12]

As shown in the figure above, the typical profile of an avalanche photo diode is doped $p^+\pi pn^+$, where π is the intrinsic drift area. In this case, photons enter the structure on top, pass through a small p^+ layer into the intrinsic area, where the photons are nearly completely absorbed. The advantages of an APD are a short response time as well as a high quantum efficiency. The lower p-region is the avalanche-zone with the highest electric field density. Due to the amplification in the avalanche diode, not only the wanted signal, but also the shot noise gets amplified [11].

2.3 Single photon avalanche diode

SPADs use the same effects as a conventional APD, including a high reverse bias. Electron-hole pairs are generated by impact ionization and the secondary electrons get drawn through the transit region where they cause further ionizations. The second process is a multiplication process as shown in Figure 3. One of the differences to normal APDs is that SPADs can be operated in Geiger mode, which means an operation above breakdown voltage. With a higher voltage the amplification can be increased up to 10^8 . In order to fulfill the requirements of a single photon detector, a high efficiency, low noise and picosecond timing jitter is needed. With a higher operating voltage, the detection efficiency increases and

the capacitance of the diode decreases. For the handling of high currents quenching is needed. This process is described in chapter 2.4. Conventional APDs cannot be used above breakdown voltage, as the dark current gets too high. With a lower breakdown voltage, the avalanche effect gets strongly damped and therefore is not usable for single photon detection. The differences between APD and SPAD are tested in chapter 3.3. For an operation above breakdown, the quality of the material has to be chosen carefully, for the dark current has to be as low as possible. A disadvantage of increasing the reverse bias voltage is an increased dark count rate. SPADs are often cooled down to reduce the dark counts and keep the SPAD at a stable temperature to obtain a stable amplification behaviour as described in chapter 2.2. The semiconductor design has to be optimized for SPADs, the p-n junction must have a uniform breakdown over the whole active area to produce current pulses with constant amplitude. Effects like micro plasma in an active area or edge breakdown can be minimized to optimize the performance of a SPAD [12] [13].

2.4 Quenching

When SPADs are operated above breakdown voltage a pulse triggered by an external photon or internal event amplifies itself. Due to this amplification effect the current grows exponentially until the space charge effect limits the current. The p-n junction is in a switched ON state, to reduce the current back to an OFF state quenching is needed. In order to quench the current different external quenching circuits can be used. This process reduces the bias voltage at least to the breakdown voltage or even lower. The quenching circuit also includes a mechanism that increases the voltage back to a level above breakdown so the diode gets sensitive again and the process can start over. In the time between the reduction of the current and restoring to a sensitive state, no photon can be detected, this is called dead time of a detector. This operation mode is called Geiger mode because of its analogy to a gas counter of ionizing radiation [13].

There are two methods to realize the quenching circuit: passive quenching (e.g. using a resistor in series to the photo diode) or active quenching. Active quenching by reducing the bias voltage may work faster and suits a very high repetition

rate. In case of a potential destruction of an expensive photo diode, a simple series resistor is a safer and easier way for quenching [13].

2.5 Gating

As described above, there is a dead-time from the pulse of an avalanche until the sensitivity is restored. This dead time is proximately in the tens of nanoseconds for SPAD used in VLC. To eliminate this effect in the best possible way when dealing with measurements in time domain, time correlated measurement is used. In a time correlated measurement the input is only enabled in a small time frame around the moment in time when a pulse is expected. This requires prior knowledge of the round trip time of the photon [14].

In the detector, the reverse bias voltage of the SPAD is switched below breakdown voltage after detecting a pulse, and is switched back above breakdown voltage right before the next light pulse is expected. The switching on and off of the SPAD and the suppression of output pulses during the switched OFF time is called gating. This time correlated measurement is done to minimize the dark counts and to provide a uniform environment for all pulses in the SPAD. By switching off the photo diode, effects like “after pulsing” or “dark counts” after the received light pulse can be ignored.

If no photons are detected and no dark count occurs during a single measurement cycle, a different mechanism has to be used to switch off the reverse bias voltage below breakdown voltage. A simple method can be used to disable the receiving state by detecting the negative edge of the gating clock. The gating of one of the used photo diodes can be seen in Figure 10 and is described in more detail in chapter 4.1.

2.6 Timing Jitter

The delay of the electrical signal and the true arrival time of the photon is not constant, but subject of statistical variation. The biggest effect causing timing jitter is found in the area where a photon set of an electron-hole pair as described below and illustrated in Figure 4. A carrier in the high field region gets accelerated

immediately, a carrier in the neutral p region has to migrate by diffusion until it reaches the depletion layer where it is accelerated by the electric field, so the pulse of this photon is detected later. The amplitude and duration of the tail are wavelength dependent, but in this application this effect can be ignored, because the light pulses emitted by a laser has a very narrow optical bandwidth and other wavelengths can be filtered out. The full width and half width maximum of the main peak can be described as statistical fluctuations. Beside longitudinal propagation in thick depletion layers (about 20 μm) also lateral propagation can dominate the diffusion of carriers. To improve the efficiency of both effects, a higher reverse bias voltage can be used. According to literature, a good timing performance can be achieved by sensing a low current level, about 100 μA , when the multiplication process is confined within a small area around the photon absorption point. [13]

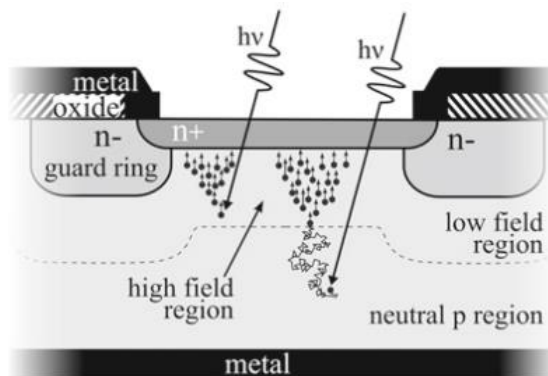


Figure 4: Timing Jitter due to absorption variance [13]

Apart from the jitter of the photo diode also semiconductors in the electronic signal processing are adding jitter to the detector.

2.7 Neutral Density Filters

ND filters or also known as OD filters can reduce the number of photons by the magnitude of decades, covering a wide spectrum starting from 350 nm to the NIR range. These filters can be made by covering a piece of glass or other transparent material with a metal layer. Metal covered filters can withstand high power, therefore they can be used with high power lasers. Stacking metal filters can cause problems because of photons bouncing between the filters. On absorptive glass

filters this problem is smaller. An ideal ND filter is wave length independent, in reality there is a wave length dependency especially at the end of the usable spectrum [15].

The factor of attenuation is related to the transmission T within a range from 0 to 1. Another more common description of the attenuation is the order of ND. Higher ND reflects more light and attenuates the light more. The relation between T and ND is represented by the following equation:

$$ND = \log_{10} \left(\frac{1}{T} \right)$$

A filter with value of ND=1 is passing 10% of the light [16].

3. Circuit Implementation

Based on the theoretical background and the existing SLR system, a circuit was implemented. A quick overview of the whole circuit is shown in Figure 5. The boundary conditions for the detection package were given on the mechanical side, so that it can fit into existing optical interfaces of the telescope. On the other side the electrical interfaces of the input trigger pulse and output pulse were given to fit the existing system. Since there are mechanical cases available with an internal dimension of 54x99x30 mm and a lens-mount on the narrow side, the detector circuit had to fit within those boundaries. A picture of the Detector assembled in the case is shown in the appendix in Figure 19.

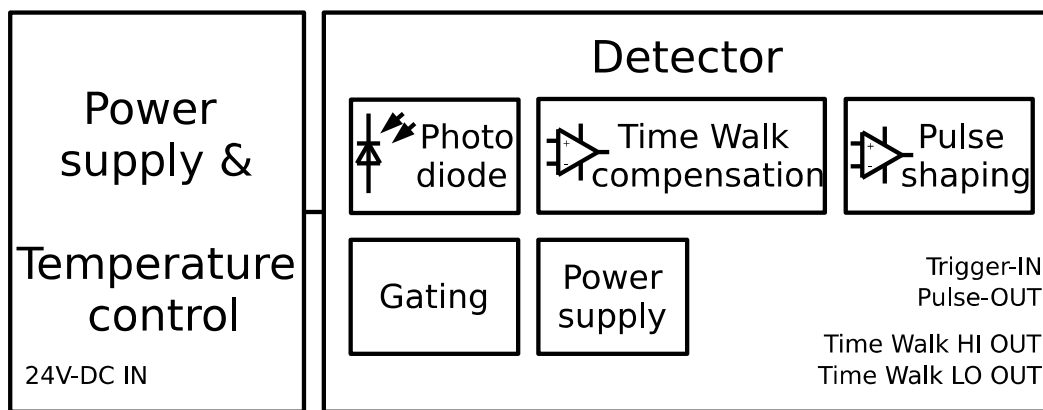


Figure 5: Simplified block diagram of the detector package

To minimize thermal drift of the detector components, stable thermal conditions are required. Due to thermal conditions and limited space the power supply was implemented separately. The thermal control is located together with the power supply because the linear current control of the thermo electric element generates additional heat and there is no need to place it near the thermo electric element itself. These two modules, the power supply with the thermal control and the detector are connected with a 9-pin D-sub connector, the pinout can be found in Table 1. On the side of the power supply the female connector is used to protect the pins against an accidental short circuit. The same principle is used on the other end of the cable. For the input of the power supply, 24 V DC is used. In general, the exact voltage at the input of the power supply is not critical as long as it stays in the operating area of the used DC/DC converters.

Table 1: Detection package cable pinout

Plug (Power Supply)	Socket (Detector)
1 high voltage	5
2 ground	2
3 cathode voltage +15V or ground	4
4 +5V supply	1
5 -5V supply	3
6 thermistor 1	8
7 thermistor 2	9
8 thermo electric element -	7
9 thermo electric element +	6

3.1 Power supply and cooling

The requirements for the power supply of the detector are as follows: symmetric voltages for the comparators as well as a high voltage source that can be adjusted over a wide range. The positive side of the symmetric supply is also used to supply the logical part of the circuit. The DC/DC converters do not require a galvanic separation, only the high voltage converter needs a galvanic separation, so that it can provide a negative voltage. During the process of development an additional voltage for the cathode with very little current, about 1mA, was needed. The second part of the requirements is the temperature control of the SPAD.

Based on an existing schematic and PCBs from colleagues at OEAW, the power supply and cooling regulation was adopted. Starting with different output voltage levels as well as additional 15V for a separate controllable cathode voltage, the changes on the power supply side are minor. For the temperature regulation the regulator was not stable in all conditions. In order to reach stability two counter measures were taken. On one hand it tended to oscillate, to prevent this behaviour, capacitors in the feedback of the operational amplifier were added. The other condition that can lead to instability was if the detector board was disconnected from the thermistor. To maintain a certain voltage at the input of the regulating amplifier, the Zener diode D1 was added.

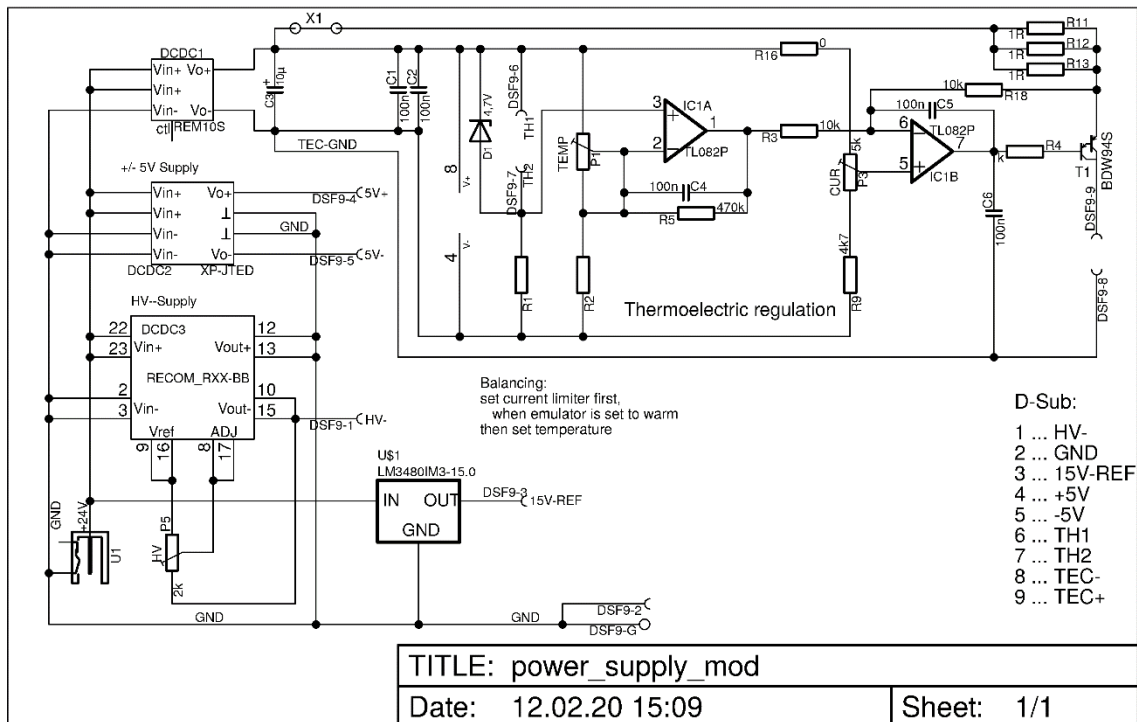


Figure 6: Power supply with temperature regulation

Different types of photo diodes have different coefficients for the thermistor. In order to match these boundary conditions the resistor values in the schematics had to be adapted. The according values are documented in Table 2.

Table 2: Resistor values for different diodes for temperature regulation

Diode	R1	R2	P1
IAG200T8	7.5k Ω	8.2k Ω	50k Ω
SAP-500	8.2k Ω	8.2k Ω	10k Ω
PGA-200	82k Ω	4.1k Ω	20k Ω

For adjusting the temperature regulator, dummy models of the photo diode are used. With the dummy models, the thermoelectric element is replaced by a power resistor and the thermistor is replaced by a potentiometer representing the same range as the thermistor. For balancing the regulator, the potentiometer of the dummy is set to a value that represents a warm temperature, then the current limiter is set according to the datasheet including some safety margin. In the second step, the dummy is set to the target temperature and the limit of the regulator is estimated to that value. After connecting the real photo diode, the regulator is

fine-tuned to the exact temperature. All these steps are performed with an ampere meter connected to the X1 connector, for normal operation the ampere meter at the X1 connector is replaced with a jumper.

The high stand-by voltage of the SPAD is set during stand-by time, when gating is OFF. The voltage can be adjusted with potentiometer P5. Voltage levels in this paragraph are given in absolute value for better understanding, since every voltage is below the cathode voltage. For the initial start-up, the high voltage is set as low as possible, therefore the voltage has to be measured on the PCB itself. To find the breakdown voltage, the photo diode is covered to block out most of the photons, so that only a few photons can hit the photo diode. Then, the voltage is slowly increased. On the one hand, the input voltage is monitored using a voltmeter to detect any problems and preventing a too high voltage. On the other hand, an oscilloscope is connected directly to the cathode of the photo diode using a 1:10 probe. Below the breakdown voltage no pulses can be seen on the cathode. When reaching the breakdown voltage, small pulses can be seen over the period of several microseconds to milliseconds, this voltage has to be noted for later usage, and the voltage is decreased by about 5 volt to be in a safe range below breakdown during standby time. Even when photons of the background light are hitting the photo diode below breakdown voltage, no pulses can be seen. The breakdown voltage is only valid for this single sample; a different photo diode of the same model has a different value for the breakdown voltage. When activating gating the pulses at the cathode are as high as the difference between the voltage above breakdown due to gating and the breakdown voltage itself, so the higher the voltage above breakdown, the higher the pulses on the cathode.

3.2 Detector

The basic detector requirements are fast gating, uniform output pulses for all detected photons, as well as measurement outputs for the development process. The detector should be usable for different kinds of SPADs. Input and output connectors are shown in Figure 5. All time-sensitive connectors are implemented as coaxial connectors, to maintain the signal shape and avoid reflections, their impedance is matched to 50Ω. Trigger-IN enables gating with a rising edge. The

falling edge can be used to disable the gate if the resistor R59 is placed as a bridge. The pulse output has a positive pulse if the SPAD gets triggered on a photon or internal breakdown. “Time Walk HI OUT” and “Time Walk LO OUT” are triggered when different voltage levels on the cathode of the SPAD are reached. These two interfaces have a negative pulse and are used for development and characterising the SPAD only. The words high and low are referring to the absolute value of the voltage, so that the low output gets triggered earlier than the high output, even if the high trigger voltage is more negative. The detailed schematic can be found in the appendix in Figure 21. To minimize the jitter difference between the LO and HI comparator as well as the thermal drift, both thermal equilibrium and production variations have to be considered. Using a package with two comparators solves both problems.

The detector is split into two parts, the PCB for analogue and for digital processing, and a small PCB for the photo diode, which is mounted perpendicular to the other PCB to face the side with the collector lens. Beside the photo diode itself, the thermistor and the thermoelectric element have to be connected to the processing board. All three parts are contained in the package of the photo diode. This package is mechanically mounted on a block of aluminium using screws. For a better thermal connection cooling paste is put between the package and the block of aluminium. To prevent a short circuit of the connectors of the package, they are protected by small plastic tubes inside of the aluminium block. As a connector for the photo diode and the thermistor a small snap-on connector makes handling easy. To obtain the signal form of the photo diode, the advantages of an RF snap-on connector suit both requirements. SMP connectors can handle over 300V and are thereby suitable for the photo diodes. On the mechanical side they can handle the misalignment from manual soldering. The only disadvantage is the maximum current they are specified to, some photo diodes are rated up to 1.5A [17], whereas the SMP connectors are only rated up to 1.3A according to their data sheets [18]. To overcome this issue soldered cables are used for the thermoelectric element.

The connectors on the opposite side of the photo diode are used to connect to the outside of the case. To simplify handling and to go without any soldered wire

that could lose connection during handling, the connectors are directly soldered to the PCB and mechanically stabilized by the case. The symmetric power supply is filtered on the detector PCB using an LC filter to provide a smooth supply for the comparators.

Controlling the gating includes the high voltage switching as well as potential output gating to prevent from output pulses when no event shall be triggered. The controlling is done by a single D-type flip-flop, it can be set and reset by the gate port as described above. If a pulse from the photo diode is detected, the gating gets disabled by the positive output pulse of one of the comparators. To decrease the high voltage even further below the breakdown voltage, in the phase of an active gating period, a charge pump is used. The capacitance can be chosen so that the charge withstands a period without any noticeable change. On the other side, the switching ON and OFF must be as fast as possible, keeping the on-gating in the range of nano seconds. In tests performed the charge pump itself is not a limitation for this process, but the capacitance of the photo diode gets a limiting factor when gating the photo diode with a differential voltage of up to 50V. Due to the capacitance and the high voltage, the switching transient is quite long in comparison to the logic elements and the transistor switching time without photo diode.

To ensure a long enough output pulse that can be detected by any kind of time measuring equipment, pulse shaping is done with a dedicated comparator where the output pulse can be used to disable the input latch for a short period of time.

3.3 Using an APD as SPAD

Single Photon Avalanche Photo Diodes are rather expensive as the cost ranges from a few hundreds (SAP500) to thousands of Euros (PGA200). Tests were performed to check if it is possible to use a conventional Avalanche Photo Diode for single photon detection. As described in chapter 2.3, SPAD are operated above breakdown voltage. The tested APD was IAG200T8 from Laser Components, a cooled down InGaAs photo diode. For the test procedure, the temperature regulation had to be adopted and tested to protect the photo diode. Light was blocked

out and cooling turned on. The measurement itself was performed with a simplified circuit as shown in Figure 7. To minimize the effects of the measuring setup a 1:10 probe was used with the oscilloscope.

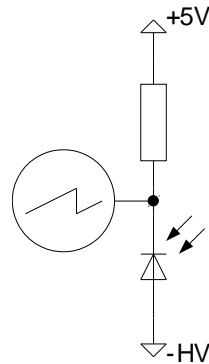


Figure 7: Simple measurements using variable high voltage and an oscilloscope

The high voltage was increased until the breakdown voltage was reached. With a higher voltage the number of small noise pulses increased but the pulses were unusable due to their small amplitude. When increasing the voltage above breakdown voltage the photo diode started to behave like a Zener diode, so the measured voltage decreased equivalent to a higher negative input voltage. The size of the measured pulses did not change at all, which shows that an APD cannot be used as a SPAD. The measured pulses are shown in Figure 8: the light pulse is hitting the photo diode at the biggest pulse that was used for triggering, all other pulses are noise.

Another test was performed with an uncooled APD from Hamamatsu, G14858-0020AA, but the results were nearly the same. In case of the Hamamatsu APD

the rapid increase of the dark current close to the breakdown voltage was documented in the datasheet.

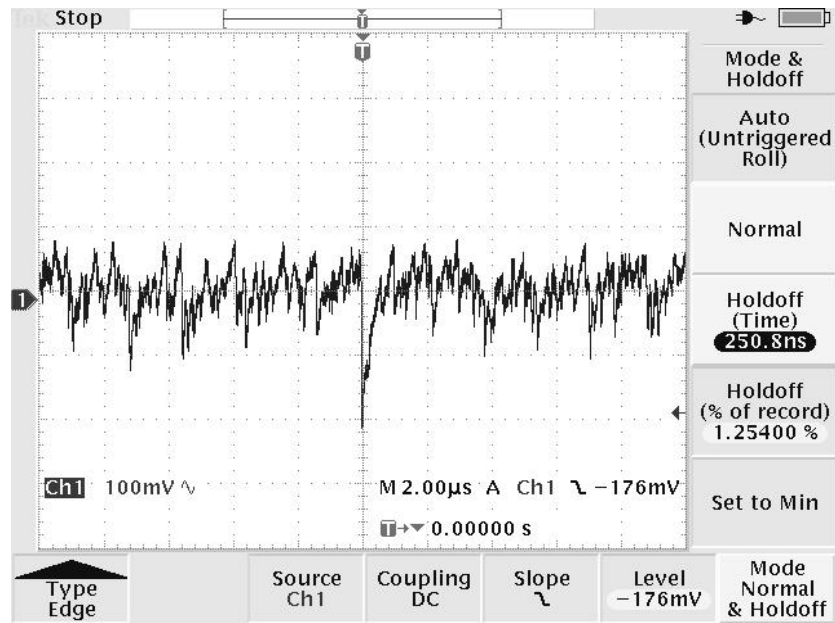


Figure 8: IAG200T8 above breakdown voltage, showing internal noise vs. external light pulse

4. Measurements

Most of the effort was put into time measurement. For measuring the time from the emission of a photon to the output of the detector a precise measurement setup is needed. With a common digital oscilloscope like the Tektronix TDS3032B used in this setup, it is not possible to make accurate time based measurements, but a rough estimation in the low nano seconds range can be done. The two high-speed channels of the oscilloscope have a timing offset slightly above one nano second between the channels. Measuring in-circuit provides a challenge of its own when it comes to maintain the original signal form and some related challenges are described in chapter 5. In spite of the precise time measurement, not every measurement cycle provides a valid result. For example, in case of a dark count the result is not in the expected time frame. Another example is a cycle without any pulse. For a representative measurement in the time domain of the output signals statistical analysis is necessary as well as the ability to save results for future usage. At Lustbuehel Observatory two types of time measurement equipment are available. Their features used during development are described below.

The SR620 Universal Time Interval Counter can measure the time between a start and a stop trigger pulse. For some measurements, the gating function is used to wait for a gate pulse before a start/stop pulse is being detected. The trigger level, the rising or falling edge, AC or DC coupling as well as the impedance can be set separately for each input port. The time resolution is between 25 ps and 50 ps, this limits the spatial resolution to 7.5 mm, according to the equation below. The SR620 is busy for 800µs after one start/stop cycle which limits the repetition rate to slightly above 1 kHz. The interval counter can be read out by the RS232 or GPIB/IEEE-488 interface, for reaching the possible 1 kHz repetition rate, the IEEE-488 interface has to be used. To connect the interface to a PC an IEEE-488 to USB adapter as well as an IEEE-488 to Ethernet adapter was used [19].

$$\frac{50 \cdot 10^{-12} s}{2} \cdot c = 7.49 \cdot 10^{-3} m$$

The other device for time measurement is the event timer A033-ET/USB by Eventech. It has a single-shot resolution with a guaranteed resolution of 5 ps and a continuous measurement rate up to $1.3 \cdot 10^6$ events per second, which leads to a maximum laser repetition rate of 750 kHz. The main difference to the time counter is, that the event timer provides the timestamp of a start or stop event. Between the events on input A and B there is a dead time of 50 ns, this has to be considered for the measurement setup. The inputs are matched to 50Ω and need NIM logic pulses with a duration longer than 4 ns and are not recommended to be longer than 40 ns to prevent channel-to-channel cross talk. NIM logic levels are negative, a logical 1 is defined from -0.6 V to -1.6 V logical 0 is 0 V. The internal 100 MHz clock is locked to an external 10 MHz reference and could be synced with a GPS receiver if an absolute time reference is needed. The interface to the PC is USB with a proprietary protocol: this can be accessed via a Windows application. Further communication can be done by TCP/IP [20].

To read out the values from the measurement devices and process these values software had to be developed. The development of the software was done in close cooperation, parallel to the hardware development, by the German bachelor student Michael Freund. The Software was written in Python3 with a platform independent approach, the used operating systems were Windows 10 and Linux (Ubuntu 18.04). Main functionalities are storage of systematic valid measurement points, as well as the visualization and statistical analysis. The software is described in more detail in chapter 4.2.

4.1 Setup

All optical components were mounted on an optical breadboard to provide the necessary mechanical stability. The different components were connected with black plastic tubes to block out any light other than the light emitted by the laser, gaps that could not be covered by any adapter were closed with black tape. For small components like the ND filters, no suitable mount was available. In order to solve this, custom mounts were 3D-printed with a tight fit on the sides of the tubes and an overlapping lid to block light from the top. The sharp wavelength filters

were directly screwed onto the lens package of the detector. A block diagram of the whole setup can be seen in Figure 9.

The lasers used in the visible spectrum were triggered by an external pulse, the detector had to be gated earlier. In this case the primary clock is a function generator and the phase shift between the laser and the gating at the detector was adjusted using an oscilloscope. For easy rebuild, the parameters used could be saved to the memory of the function generator. The timing can be seen in Figure 10, channel 1 is the time walk LO output of the detector, channel 2 is the function generator triggering the laser, channel 3 is the voltage directly at the cathode of the photo diode and channel 4 is the output of the function generator triggering gating of the detector. When gating is triggered, the anode voltage is decreased by 50V and the capacitance of the photo diode also decreases the voltage at the cathode. This effect can be seen in the centre of the scope at channel 3. When using the photo diode PGA200 for 1064 nm instead of the SAP500 for visible light, the voltage is decreased only by 10V to prevent a destruction of the photo diode.

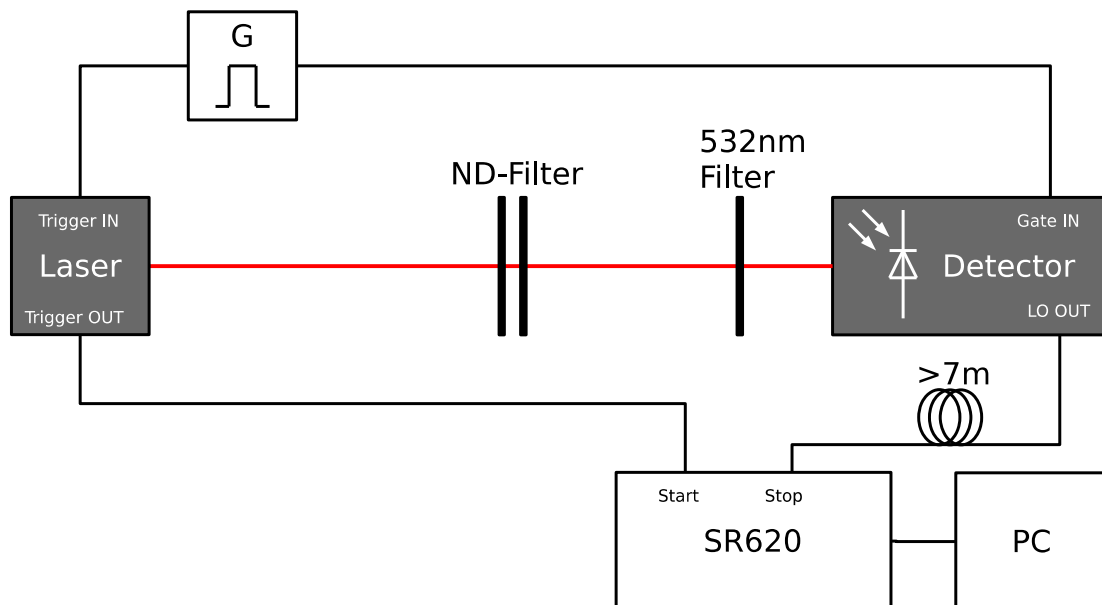


Figure 9: Setup for absolute time walk measurement

For time measurement the input trigger of the laser could not be used, since the time between the input signal and the actual light pulse changed with the temperature of the laser and had a huge jitter in general. Depending on the laser, there

is an output pulse for measurement, directly triggered by the photons transmitted by the laser. In order to overcome the dead time of the SR620 between the start and stop pulse, the stop pulse from the detector was delayed by the use of additional 7m coaxial cable. Including the velocity factor of RG-58 cable this leads to a time delay above 30ns.

When measuring the time with the event timer A033-ET, the setup is nearly the same, except that the signals for the event timer had to be adjusted to NIM logic levels using coaxial adapters like pulse inverters and 50Ω termination adapters. A disadvantage of the event timer were missing features like gating or triggering input so that the measurement was only valid after a separated signal. The fixed input levels that increased the complexity of the measurement setup were another downside. The gating function is a big improvement when measuring the relative time walk, described in chapter 5. To overcome the longer dead time between the inputs a long coaxial cable was used.

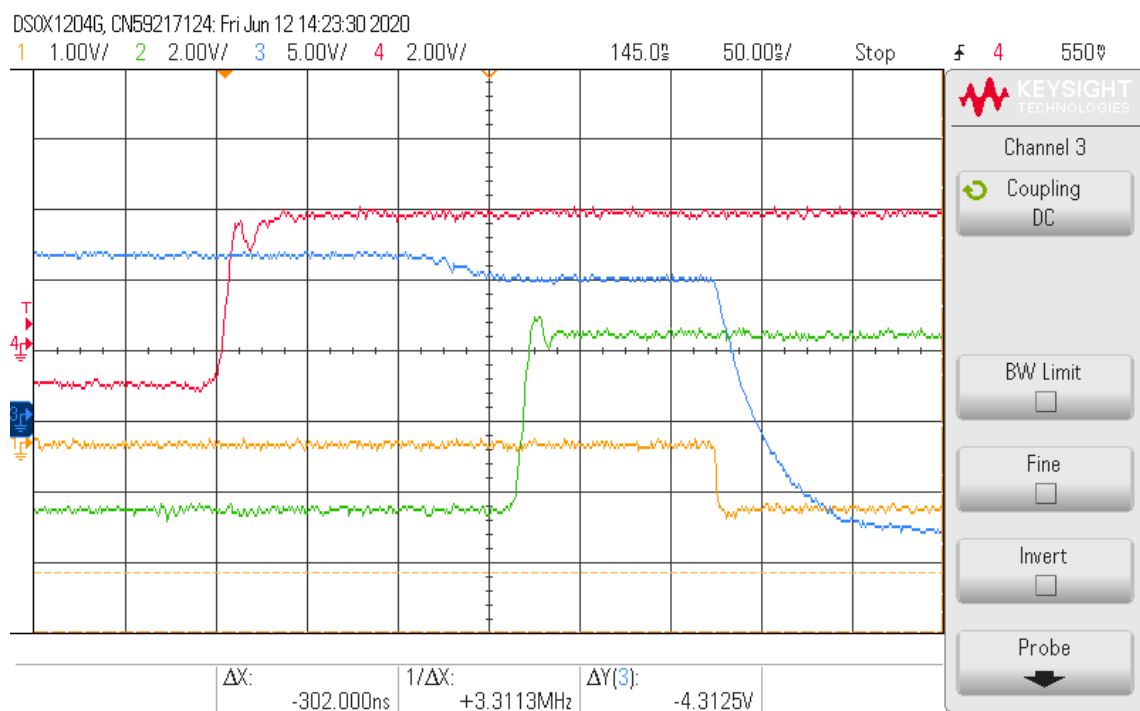


Figure 10: Timing on the SAP500

4.2 Software

The software was developed in parallel to the detector prototype to process the measured time intervals with a semi-automatic procedure. The start of the measurement for a set of N start/stop cycles as well as the post processing in the software is the same for the interval counter SR620 as well as the event timer A033-ET. Because of the different hardware interfaces it is split into two different python programs. The graphical interface can be seen in Figure 11; to fit the printed page, buttons for saving and loading measured data are cut out. In the centre of the window is the diagram showing the measurement points. On the x-axis, the single measurement cycles are plotted, and on the y-axis the time of each single measurement cycle. In case of the measurement shown below, all the detected photons are below 100 ns and the points filling the diagram are dark counts. Cutting out the noise offside the interesting part, can be done by hand or by using a cut function based on a sigma distribution. All statistical parameters can be adjusted in the settings. If there are only interesting points left, the statistics can be calculated. The result is printed to the right side of the window. Calculated parameters include the mean value, standard deviation, RMS, difference between peak value and mean as well as skew and kurtosis. In Figure 11 the calculated values are based on the values to the bottom of the plot and not to the visible area. To estimate the detected pulses the number of visible data points is printed on the top left. For an easy measurement procedure the raw data as well as the calculated statistics can be exported into the data directory of the program. If there is already a file with the same filename, a counter is appended to the filename to avoid overwriting the data. The statistics are appended to a single file, referring to the raw data file. The exported files are ASCII files with delimiters for automatic processing. For a quick handling of the functions the buttons have shortcuts. If the mouse is held over a button for a longer period, the shortcut is displayed.

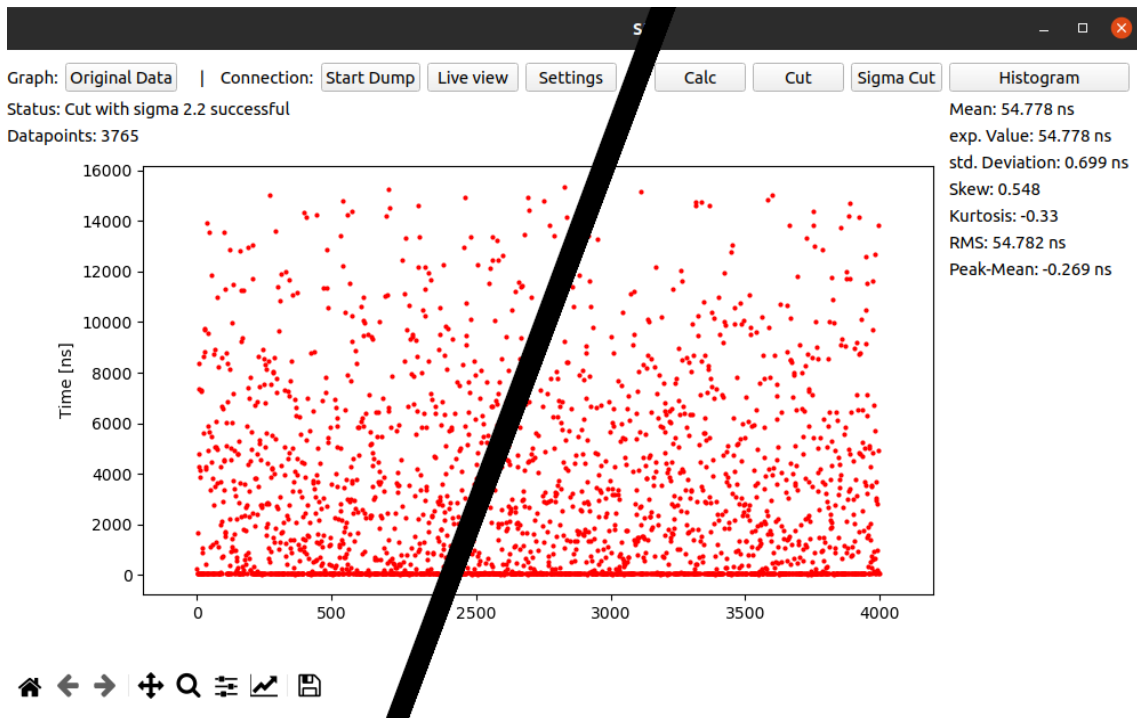


Figure 11: Measurement software by Michael Freund, with cut out section to fit the page.

Some functions, like the measuring process or the calculation of the statistics may need some time. The program status is printed to the top left, displaying if the program has already finished a specific task. Besides the cutting in time domain, the diagram provides features for zooming, moving and image export. The buttons for these functions are located on the bottom left. For a quick estimation of the distributed measurement points a histogram can be used. Although some features are not available during live view it is possible to optimize the timing regarding the interval counter or event timer. Another use case of the live view function is to optimize the rate of detected photons based on the optical setup.

4.3 Time measurement

Most of the measurements were made over a period of 4000 start-stop cycles. If the gating is activated and no laser pulse is detected, the cycle gets stopped with the next start cycle, even when all photons are blocked out. This occurs in less than one percent of the cycles using the SAP500 photo diode. If no photons are detected, most of the output pulses are spontaneously generated in the photo diode due to dark counts.

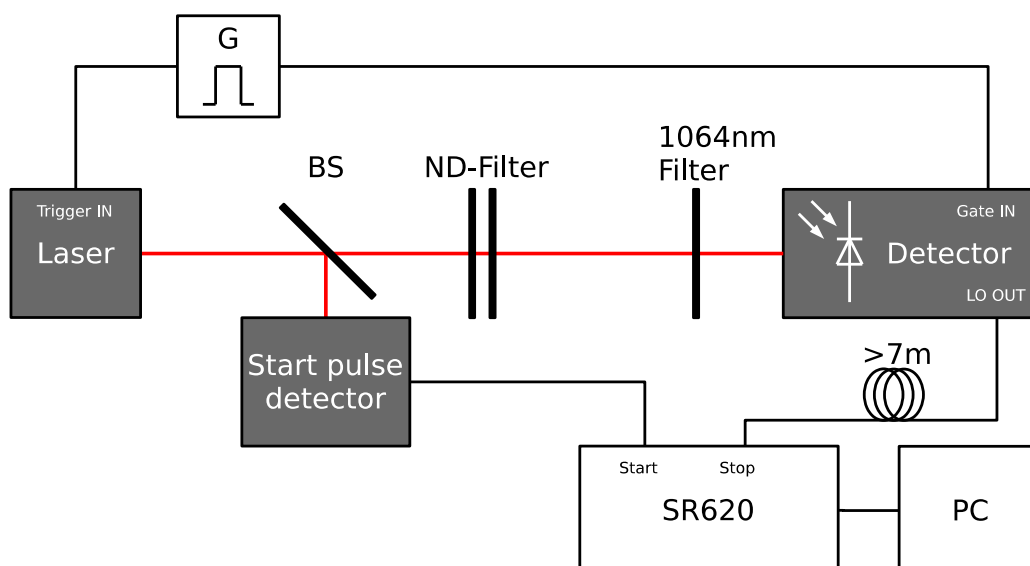


Figure 12: Block diagram with beam splitter and external start pulse detector

For 1064 nm the used laser did not provide an electrical start pulse. A beam splitter with a photo diode for start pulse detection was built. As beam splitter a reflective ND-filter was placed in a 45 angle to the laser beam, in order to hold all components in place and providing an enclosure that blocks all light from the outside, the case was 3D printed. The parallel shift due to the beam splitter was no problem, since the detector had a collimating lens with the photo diode in the focus point.

4.4 Time Walk

Based on the setup above the time between laser pulse start and the LO output of the detector was measured and the number of photons transmitted to the detector was regulated by the use of ND filters. For time walk measurement the used laser Hamamatsu Picosec light pulser PLP-01 was in the red spectrum instead of the target wavelength of 532 nm, because it was the only non-stationary laser available with a short pulse length in the range of 30 ps. The energy of photons changes with the wavelength, it is unclear if there is a considerable difference in the time walk for different wavelengths.

Table 3: Absolute time walk SAP500, Hamamatsu Picosec light pulser PLP-01

ND-Filter	Exp. Value	Time walk	Std. Deviation	Return rate
	ns	ns	ns	
ND0	52.628	0.000	0.045	3912/4000 (97.8 %)
ND1	53.288	0.660	0.126	3902/4000 (97.6 %)
ND2	54.306	1.678	0.527	3528/4000 (88.2 %)
ND3	54.819	2.191	0.749	1266/4000 (31.7 %)
ND4	54.980	2.352	0.765	194/4000 (4.85 %)
ND5	54.963	2.335	0.682	29/4000 (0.73 %)

From a high return rate of 97.8 % without an ND filter to a return rate about 0.73 %, the expectation value of the received pulses changes with the number of photons hitting the detector. This decreases the possible spatial resolution of the detector as it is unknown how many photons are hitting the sensor for one pulse. A visualisation of the received pulses can be found in Figure 22, the appendix for ND0 and in Figure 23 for ND5. In all measurements the detected pulses outside the expected range were cut out, so only the pulses used for the statistic calculation are visible in the figures. With a lower number of photons the standard deviation is increasing. A visualisation of the measurement in Table 3 can be seen below in Figure 13.

With a high ND filter of ND5 the standard deviation decreases, which is most likely due to the small amount of photons detected. In the laboratory measurement setup the dynamic range of the number of photons per pulse was higher than in a realistic SLR system, with a dynamic range of the order of 1 to 10^3 photons per pulse, so the measurement error in a real system would be not as high as in the laboratory.

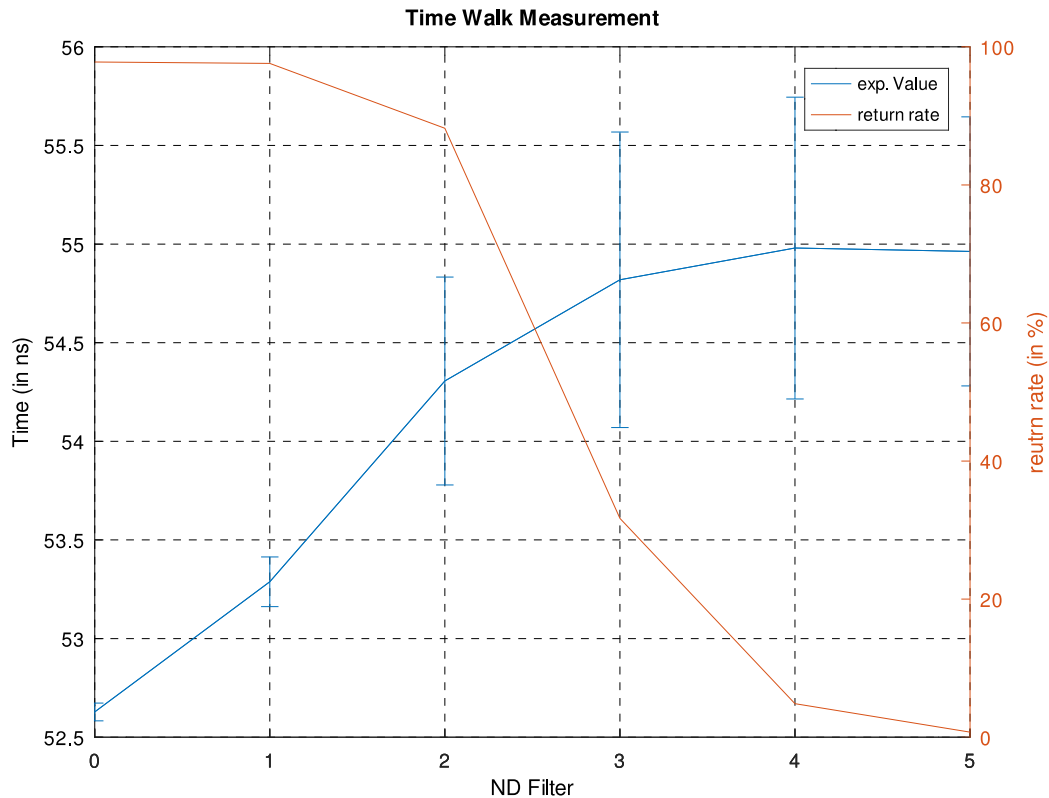


Figure 13: Absolute Time walk measurement without compensation

4.5 Measuring at 1064 nm

The detector circuit for 1064 nm was tested using the SPAD PGA500. The analogue parameters were optimized for this photo diode, including a small gating voltage for the anode as well as the voltage for the cathode. To protect the photo diode against accidental destruction a separate power supply and PCB was built using the same PCB design as for the detector for the visible spectrum.

For testing the 1064 nm detector the available laser had no output pulse for measuring, so the setup shown in Figure 12 was used. At the time of a working detector for 1064 nm no non-stationary pico second laser for 1064 nm was available, so basic tests were performed using a nano second laser. Using a longer laser pulse allows to check the basic functionality of the circuit and a basic adjustment for the different voltage levels including the pulse discrimination described in chapter 5. With a long laser pulse it is not possible to make time walk measurements in a range shorter than the duration of the laser pulse.

5. Time Walk compensation

After determining the time walk in the previous chapter, this measurement uncertainty should be minimized as far as possible. The theory behind the compensation is an energy dependent rise time of the pulse at the SPAD, and therefore also a rise in the number of photons [21]. This principle is shown in the figure below for a different type of SPAD. In this case a precise measurement with an oscilloscope would be quite difficult as the photo diode used (SAP500) has a high dark count rate.

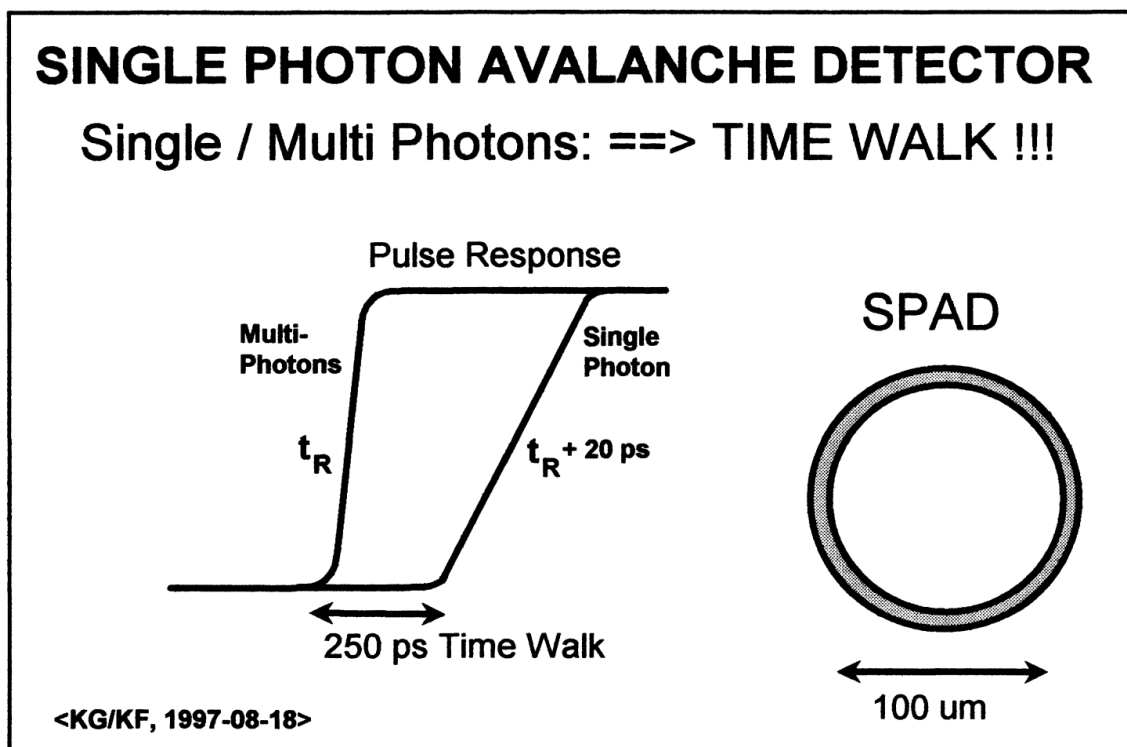


Figure 14: SPAD pulse with visualisation of the time walk [21]

According to the theory above, a pulse with a smaller energy gets detected later, this has been verified in chapter 4.4. Additionally the rise time should be slower. In the previous measurement the trigger was set to the bottom of the figure above. To check if the theory about the rise time also applies to the used SAP500, a second measurement trigger was set at a higher level. In the used circuit the higher level is more negative than the lower level. The term of the time walk at the low level is referred to as absolute time walk; the difference between the low

and the high trigger is referred to as relative time walk. In order to verify the dependency on the rise time a setup similar to the setup shown in Figure 9 was used. For the start pulse the low measurement output was used instead of the laser, and for the stop pulse the high measurement output. To synchronize the time measurement with the SR620 the gate function was enabled, and only pulses after a gating pulse were detected. As gating pulse, the laser output pulse was used. In previous measurements the whole measurement setup and the circuit itself had a longer time delay between start and stop pulse. To overcome the dead time of the SR620 between start and stop pulse, an additional coaxial cable was used. Because of the fix length of the additional coaxial cable, the measured time will be shifted in time domain; as the measurements are only relative to each other during one measurement cycle, this is no problem.

Table 4: Relative time walk SAP500, Hamamatsu Picosec light pulser PLP-01

ND-Filter	Exp. Value	Time walk	Std. Deviation	Return rate
	ns	ns	ns	
ND0	51.098	0.00000	0.036	3838/4000 (96.0 %)
ND1	51.164	0.06600	0.037	3903/4000 (97.6 %)
ND2	51.205	0.10700	0.039	3608/4000 (90.2 %)
ND3	51.234	0.13600	0.057	1689/4000 (42.2 %)
ND4	51.316	0.21800	0.100	1170/4000 (29.3 %)
ND5	51.339	0.24100	0.092	1024/4000 (25.6 %)

As shown in Table 4, the relative time walk increases when adding more ND filters to the setup. This setup cannot be used to quantify the relative time walk in the low or single photon range, as the detected pulses cannot be correlated to their source. For example for ND3 and higher order of filters the number of detected pulses in the expected range is way higher than those measured in the absolute time walk. It is unknown if a detected pulse is due to dark counts or photons from the laser source. As visual example, two plots of the relative time walk measurement are available in the appendix.

5.1 Concept

The concept of compensating the absolute time walk is to use the detectable relative time walk. The basic circuit diagram for compensation is shown below in Figure 15. It is split into three sections, the comparators for detection the threshold summarized as pulse discrimination, the passive adjustment of the voltage levels and the timing and the compensation itself. In the prototype there was another stage at the output, which was used only to get an optimal output pulse.

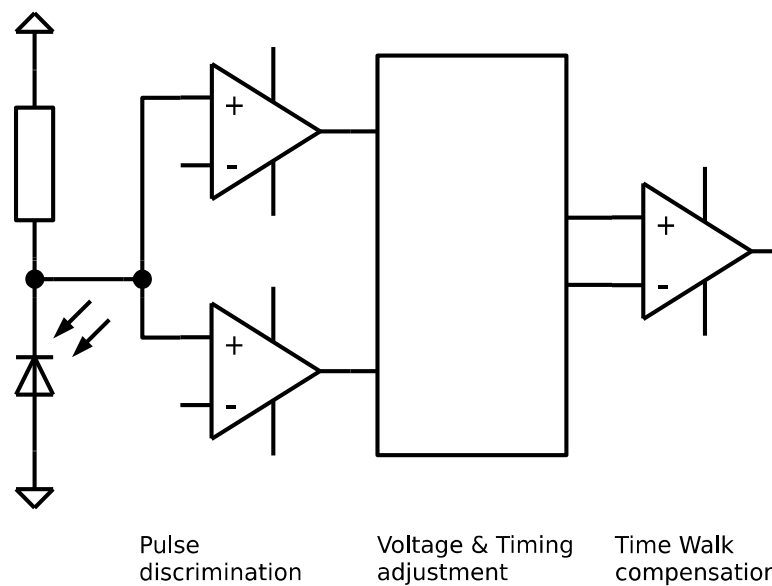


Figure 15: Circuit diagram for time walk compensation

The voltage levels at the output of the pulse discrimination stage are adjusted, so that the two pulses intersect each other in the way visualized in Figure 16. The edge of the HI pulse is activating the comparator used for time walk compensation. If the HI pulse gets triggered later the comparator is activated earlier. By adjusting the gradient of the pulse as well as the differential level the compensation process can be fine-tuned.

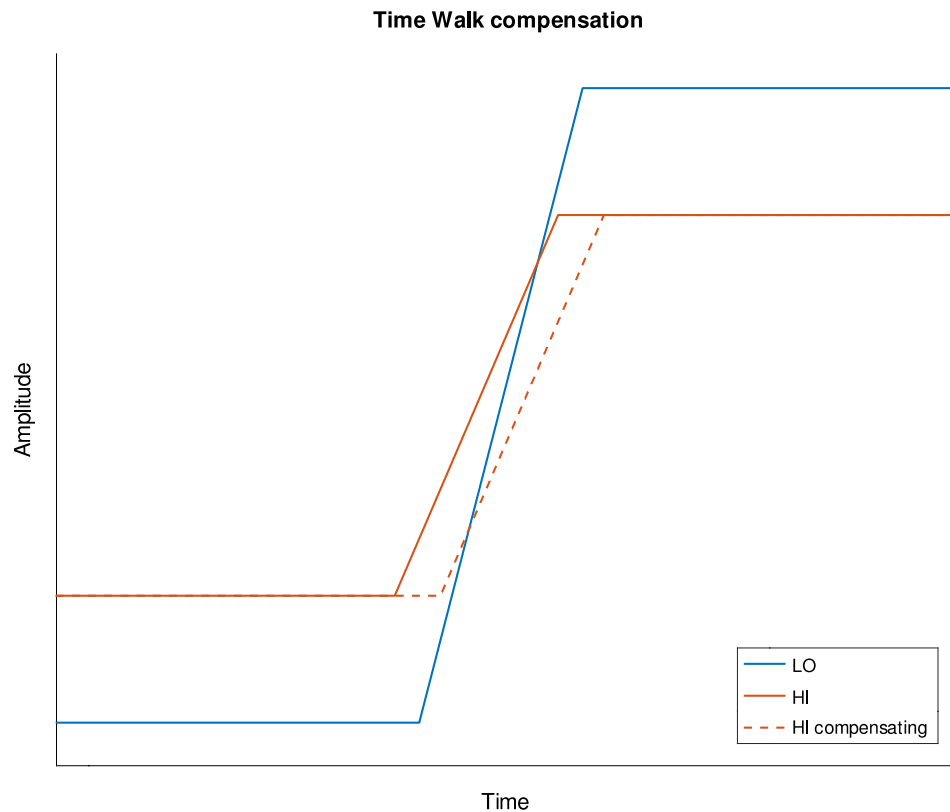


Figure 16: Concept for time walk compensation

5.2 Delay Line

The LO (blue) pulse shown in Figure 16 gets triggered before the HI pulse (red). To make a compensation possible the LO pulse needs to be delayed. For that purpose, a delay line was layouted on to the PCB. During the process of adjusting the delay for the SAP500 it became clear that the delay line was too short for the long delay. To overcome this issue, in the best way possible a piece of wire was added. Due to the time shift of the different channels at the oscilloscope a precise time measurement of the time difference was not possible. Fine-tuning was done empirically, and the measurement for Figure 17 was done by saving two separate measurements and plotting them into one plot.

The quantity of relative time walk can be adjusted by changing the trigger voltage of the HI comparator. The voltage level was set by the maximum usable delay line without distorting the signal.

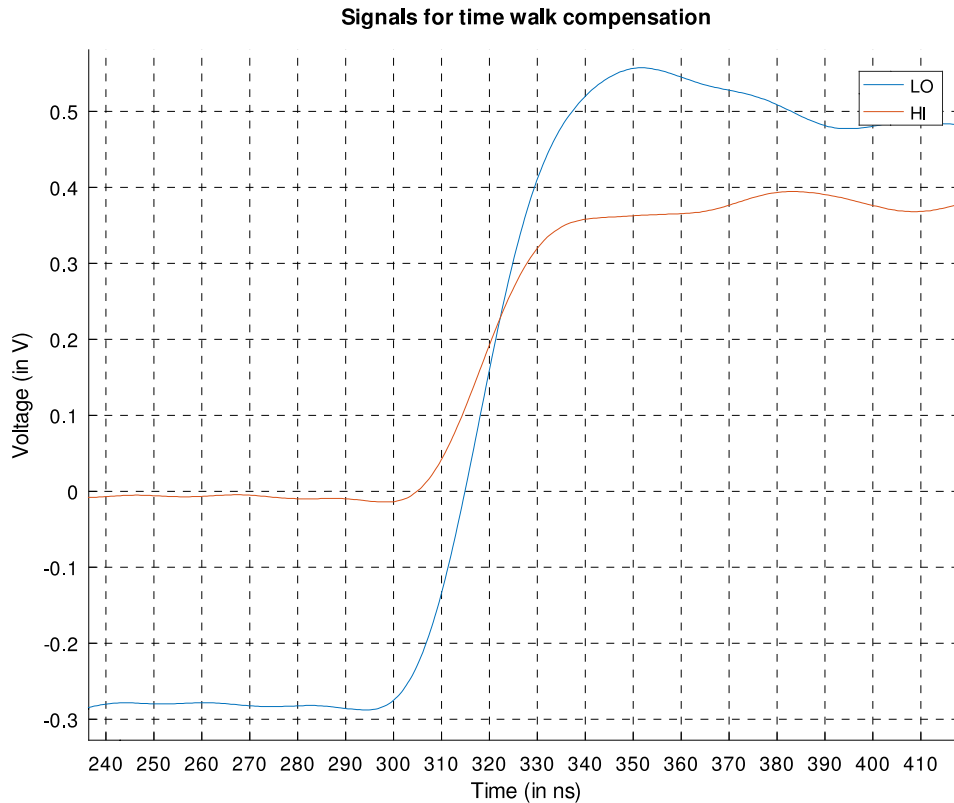


Figure 17: Adjusting timing for time walk compensation

5.3 Measurements

With the time walk compensation optimized as described above, the output pulse with compensation of the time walk was measured again by the same variation of the ND-filters. The measurement setup was the same as for the absolute time walk with the difference that the output of the detector is the compensated pulse output instead of the measurement LO output directly at the pulse discrimination. The detailed measurement results of the time compensated output can be found in Table 5 Based on the return rate ratio of the uncompensated measurement (absolute time walk in Table 3) and the compensated time walk measurement, the results comparing the different measurements can be found in Figure 18.

Table 5: Compensated time walk SAP500, Hamamatsu Picosec light pulser PLP-01

ND-Filter	Exp. Value	Time walk	Std. Deviation	Return rate
	ns	ns	ns	
ND0	84.884	0.000	0.061	3803/4000 (95.1 %)
ND1	85.434	0.550	0.115	3804/4000 (95.1 %)
ND2	86.449	1.565	0.551	3383/4000 (84.6 %)
ND3	86.854	1.970	0.674	1073/4000 (26.8 %)
ND4	86.924	2.040	0.683	193/4000 (4.83 %)
ND5	86.659	1.775	0.893	28/4000 (0.70 %)

The time walk changes over the return rate with the biggest time walk in the area with a high amount of photons and small change in the range of a lower return rate. Developing a simple model describing the time walk over the whole range was not possible. When looking to the plot based on the ND filters (Figure 13) a linearization over the ND filters can be done from ND0 to ND3. As the ND filters are reducing the number of photons on a logarithmic scale, the relationship between the absolute time walk and the number of photons is exponential. It is not clear why the ratio between the time walk and ND filters changes with a higher number of ND. In order to reach an ND above ND3, filters were stacked with a few millimetres distance in between and in a decreasing order. Because the ND filters used reflect photons back, the photons will be reflected again in the direction of the detector by a previous filter. Therefore the observed effect could be caused by the stacking of the ND filters. An argument supporting this theory is that the return rate is not decreasing as fast as expected for a higher ND.

Time walk compensation was bigger in the range of lower return rate. A possible explanation for the reduced time walk in the sub one percent return rate could be a measurement error due to the small sample size combined with a big standard deviation.

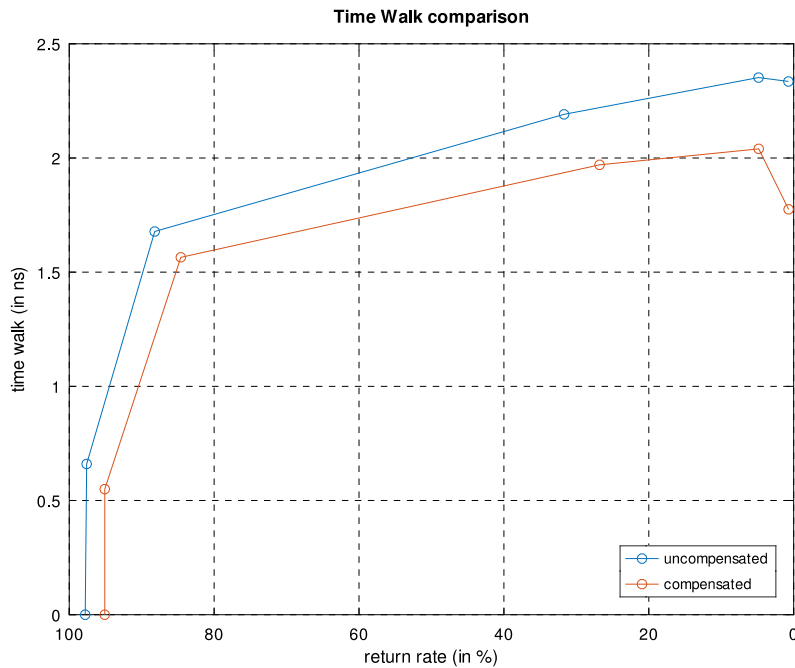


Figure 18: Time walk comparison

After testing the detector in a laboratory setup, the next step was a verification in a real SLR system. The test was performed by a colleague at the Lustbuehel Observatory. Therefor the detector was mounted onto the telescope and was integrated into the SLR measurement setup. For the time walk test, the telescope was pointed to the in-house calibration target, the amount of photons was reduced in two steps. A measurement with a high number of photons is difficult, as single scattering photons may trigger the detector too early. When comparing the measurement in the real SLR system (Table 6) with the compensated measurements in the laboratory (Table 5), the detector performs even better in the real SLR system for the measured parameters, time walk and standard deviation.

Table 6: Time walk in real SLR setup using SAP500, pointed at calibration target

ND-Filter	Time walk	std. Deviation	return rate
	ns	ns	
ND0	0	0.68	100 %
ND3	918	0.200	4 %

6. Conclusion and Outlook

The task for this thesis was to develop a generic prototype for a photon detector that can be used in an SLR system. The prototypes for visible light and 1064 nm were tested and when possible the performance determined.

6.1 Conclusion

With the developed prototype it is possible to reliably detect photons and minimize noise like dark counts based on a coherent measurement. The detector circuit can be generically used for different SPADs and the voltages as well as the pulse discrimination can be adopted with potentiometers or by changing the values of the used components. The measurement uncertainty that is due to the number of photons can be compensated in a small scale.

Using the SPAD SAP500 for the visible spectrum instead of the PGA200 for the near infrared spectrum in the process of development has the advantages of being cheaper and off-the-shelf available. Especially during development another advantage had to be considered, that is that the SAP500 is more resistant to over-voltage or over-current. The downsides of the SAP500 are a high dark count rate and a high jitter in the single photon range.

The design of the gating process of the photo diode using a charge pump instead of using a permanent power supply that is switched on and off, has the side effect to protect the photo diode against destruction. If in a case of failure the gating is not disabled the photo diode will not be destructed by a permanent voltage above breakdown as the gating stops when the stored charge is used up.

6.2 Future improvements

During the design process wires were used to connect the thermoelectric element with the main PCB as the maximal current of the thermoelectric element is higher than the maximum current of the used SMP connectors. After testing the whole cooling setup, it became clear that a current slightly above 1A is enough. So to

make the handling of the two PCBs even easier, the soldered wire could be replaced by an SMP connector. In order to compensate the time walk even better a longer delay line is needed, which includes an extension to the bottom of the PCB. For a longer delay line an in-circuit impedance matched microstrip is required to maintain the signal form of the pulse. Therefore, the PCB layout should be changed from two to four layers. To verify if the effects observed in the high ND range are due to the stacked ND filters, single high ND filters could be used.

Finally, to measure and optimize the time walk of the PGA200 a 1064 nm picosecond laser is required. The proceeding is similar to the steps described in the thesis. In general PGA200 makes measurements easier, as there are fewer dark counts.

Bibliography

- [1] „International Earth Rotation and Reference System Service,“ [Online]. Available: <https://www.iers.org/iers/EN/Science/Techniques/slr.html>. [Accessed 31 03 2020].
- [2] N. S. G. Program, „Satellite Laser Ranging and Earth Science“.
- [3] „Lunar Laser Ranging (LLR), International Laser Ranging Service,“ [Online]. Available: <https://ilrs.gsfc.nasa.gov/science/scienceContributions/lunar.html>. [Accessed 02 04 2020].
- [4] G. Kirchner und F. Koidl, „Infrared Laser Ranging to Space Debris - a chance for ILRS; Synergies between SLR and orbital debris,“ 10 2014. [Online]. Available: https://ilrs.gsfc.nasa.gov/ilrw19/docs/2014/Presentations/3009_Kirchner_presentation.pdf. [Accessed 01 04 2020].
- [5] D. T. Kelso, „Supplemental Two-Line Element Sets,“ CelesTrak, [Online]. Available: <https://celestrak.com/NORAD/elements/supplemental/>. [Accessed 01 03 2020].
- [6] D. T. Kelso, „Frequently Asked Questions: Two-Line Element Set Format,“ CelesTrak, [Online]. Available: <https://www.celestrak.com/columns/v04n03/>. [Accessed 01 03 2020].
- [7] „International Laser Ranging Service, Ground Segment,“ [Online]. Available: <https://ilrs.gsfc.nasa.gov/technology/groundSegment/index.html>. [Accessed 30 03 2020].
- [8] U. Tietze, C. Schenk und E. Gamm, Electronic Circuits, Handbook for Design and Application, Springer, 2002.
- [9] A. Kitai, Principles of Solar Cells, LEDs and Diodes, John Wiley & Sons Ltd., 2011.
- [10] G. Litfin, Technische Optik in der Praxis, Springer, 2005.
- [11] W. Harth und H. Grothe, Sende- und Empfangsdioden für die Optische Nachrichtentechnik, Springer, 1998.

-
- [12] Laser Components, „single photon avalanche diodes,“ [Online]. Available: https://www.lasercomponents.com/fileadmin/user_upload/home/Datasheets/lc/publications/single-photon-avalanche-diodes.pdf. [Accessed 24 02 2020].
- [13] T. Lucarorto, A. C. Parr und K. Baldmin, Single-Photon Generation and Detection, Physics and Applications, Elsevier, 2013.
- [14] L. Zhang, D. Chitnis, H. Chun, G. Faulkner, D. O'Brien und S. Collins, „A Comparison of APD- and SPAD-Based Receivers for Visible Light Communications,“ *Journal of Lightwave Technology (Volume: 36)*, pp. 2435-2442, 12 06 2018.
- [15] D. W. Becker, Advanced Time-Correlated Single Photon Counting Techniques, Springer, 2005.
- [16] Thor Labs, „IR Reflective ND Filters,“ Thor Labs, [Online]. Available: https://www.thorlabs.com/newgrouppage9.cfm?objectgroup_id=6007. [Accessed 17 02 2020].
- [17] „SAP 500, Datasheet,“ Laser Components, [Online]. Available: https://www.lasercomponents.com/fileadmin/user_upload/home/Datasheets/lc-apd/sap-series.pdf. [Accessed 10 02 2020].
- [18] „Technical Datasheet, SMP connector,“ [Online]. Available: https://products.rosenberger.com/_ocassets/db/19S103-500L5.pdf. [Accessed 10 02 2020].
- [19] Stanford Research Systems, MODEL SR620 Universal Time Interval Counter, Sunnyvale, California, 2019.
- [20] J. M. Serna und B. Vaquero, „EVENT TIMER A033/USBAND SYNCHRONIZATION SYSTEM LANTIME M3000, Event Timer –Time & Frequency Systems(specifications and setup instructions),“ Guadalajara, 2019.
- [21] G. Kirchner, F. Koidl, K. Blazej, K. Hamal und I. Prohazka, „Time Walk Compensated SPAD: Multiple Photons Versus Single Photon Operation,“ *SPIE Vol. 3218*, pp. 106-112, 1997.

List of Figures

Figure 1: Simple block diagram of a SLR system.....	10
Figure 2: Energy levels in a photo diode [9]	13
Figure 3: Function principle of an APD [12].....	14
Figure 4: Timing Jitter due to absorption variance [13]	17
Figure 5: Simplified block diagram of the detector package	19
Figure 6: Power supply with temperature regulation	21
Figure 7: Simple measurements, variable high voltage and an oscilloscope ...	25
Figure 8: IAG200T8 breakdown voltage, internal noise vs. external light.....	26
Figure 9: Setup for absolute time walk measurement	29
Figure 10: Timing on the SAP500	30
Figure 11: Measurement software by Michael Freund, with cut out section	32
Figure 12: Block diagram with beam splitter and external start pulse detector	33
Figure 13: Absolute Time walk measurement without compensation.....	35
Figure 14: SPAD pulse with visualisation of the time walk [21]	36
Figure 15: Circuit diagram for time walk compensation.....	38
Figure 16: Concept for time walk compensation	39
Figure 17: Adjusting timing for time walk compensation	40
Figure 18: Time walk comparison	42
Figure 19: Detector with open case.....	51
Figure 20: Detailed power supply with temperature regulation	52
Figure 21: Detailed circuit diagram.....	53
Figure 22: Absolute time walk SAP500, ND0	54
Figure 23: Absolute time walk SAP500, ND5	55
Figure 24: Compensated time walk SAP500, ND0.....	56
Figure 25: Compensated time walk SAP500, ND5.....	57

Figure 26: Relative time walk SAP500, ND0	58
Figure 27: Relative time walk SAP500, ND4	59

List of Tables

Table 1: Detection package cable pinout	20
Table 2: Resistor values for different diodes for temperature regulation	21
Table 3: Absolute time walk SAP500, Hamamatsu light pulser PLP-01	34
Table 4: Relative time walk SAP500, Hamamatsu light pulser PLP-01	37
Table 5: Compensated time walk SAP500, Hamamatsu light pulser PLP-01 ..	41
Table 6: Time walk in real SLR using SAP500, pointed at calibration target....	42

List of Abbreviations

APD.....	avalanche photo diode
LLR	Lunar Laser Ranging
ND.....	Neutral Density
OD.....	Optical Density
OEAW	Austrian Academy of Sciences
PCB.....	printed circuit board
RF	radio frequency
SLR	Satellite Laser Ranging
SMP	sub miniature push-on
SPAD	single photon avalanche diode
TCP	Transmission Control Protocol/Internet Protocol
TLE	Two Line Element
VLC	visible light communication

Appendix



Figure 19: Detector with open case

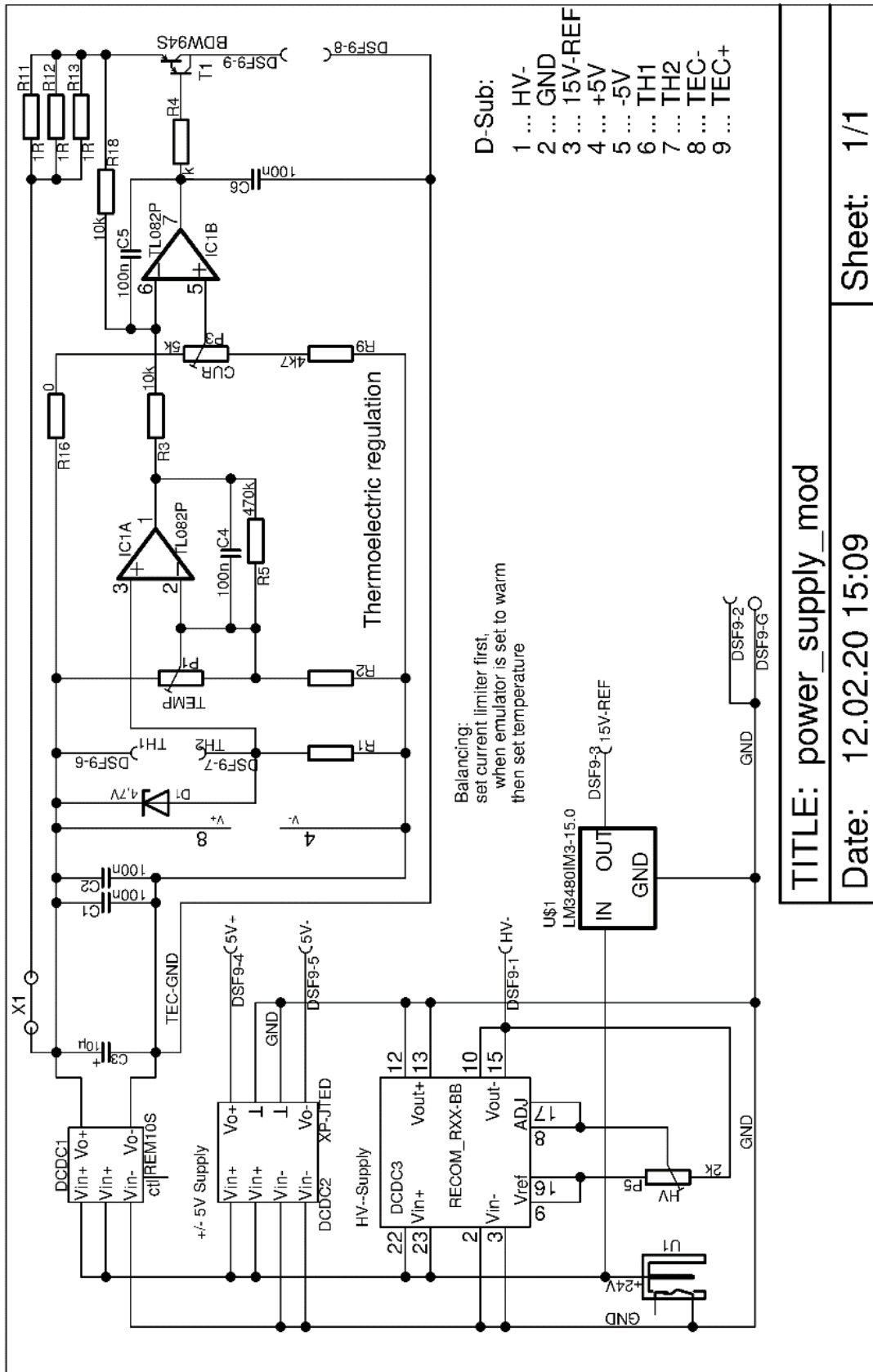


Figure 20: Detailed power supply with temperature regulation

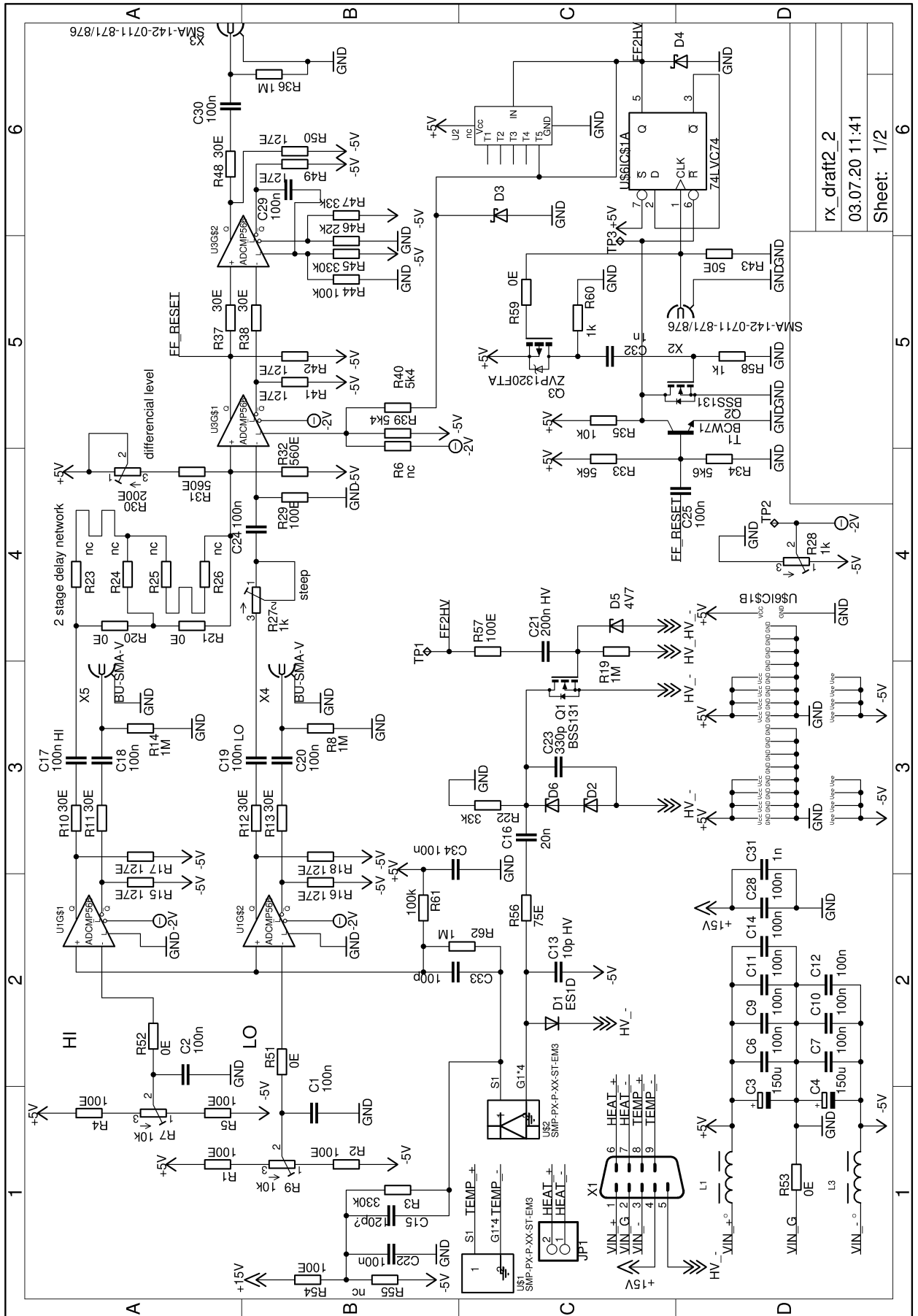


Figure 21: Detailed circuit diagram

Mean: 52.628 ns
 exp. Value: 52.628 ns
 std. Deviation: 0.045 ns
 Skew: 0.046
 Kurtosis: 0.064
 RMS: 52.628 ns
 Peak-Mean: -0.013 ns

Status: Calculation successful
 Datapoints: 3912

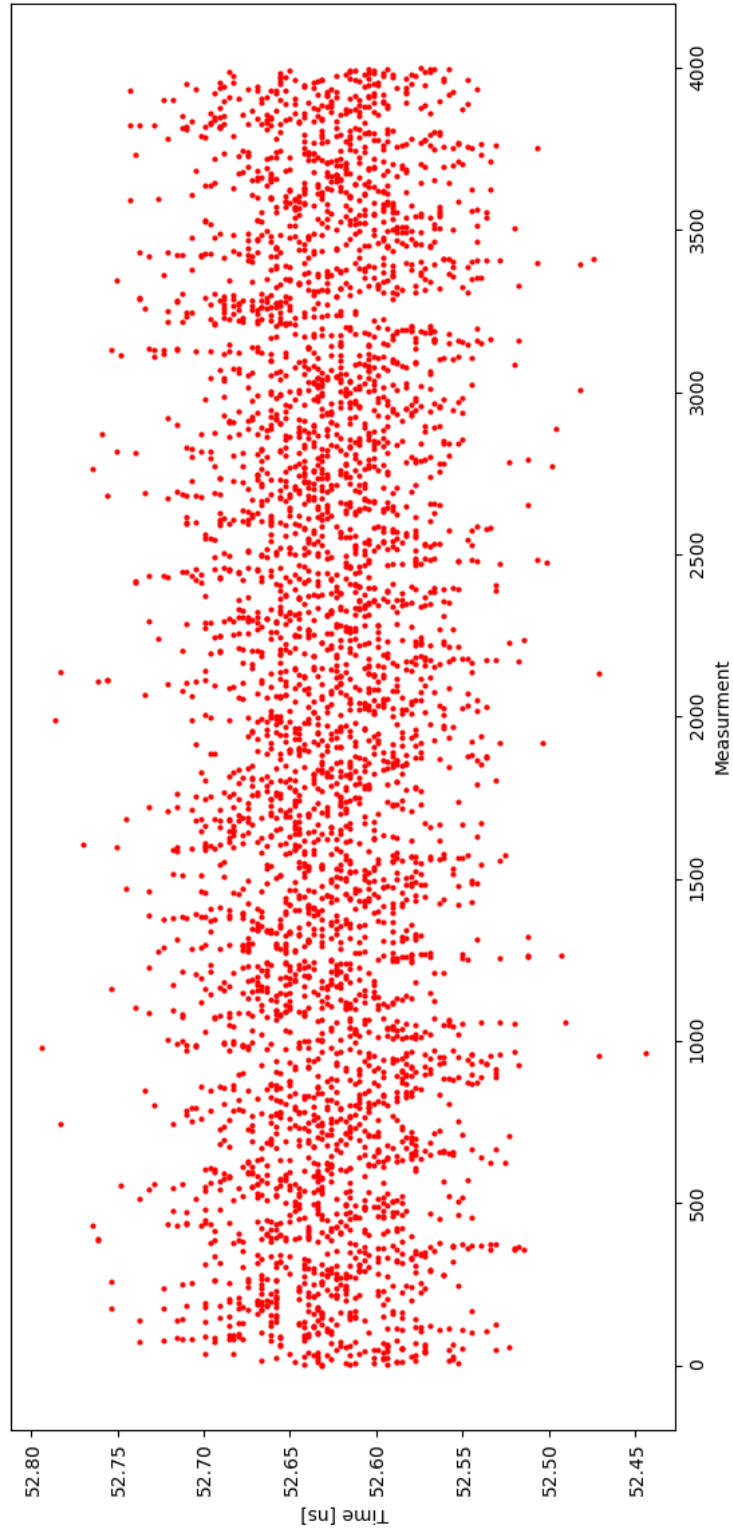


Figure 22: Absolute time walk SAP500, ND0

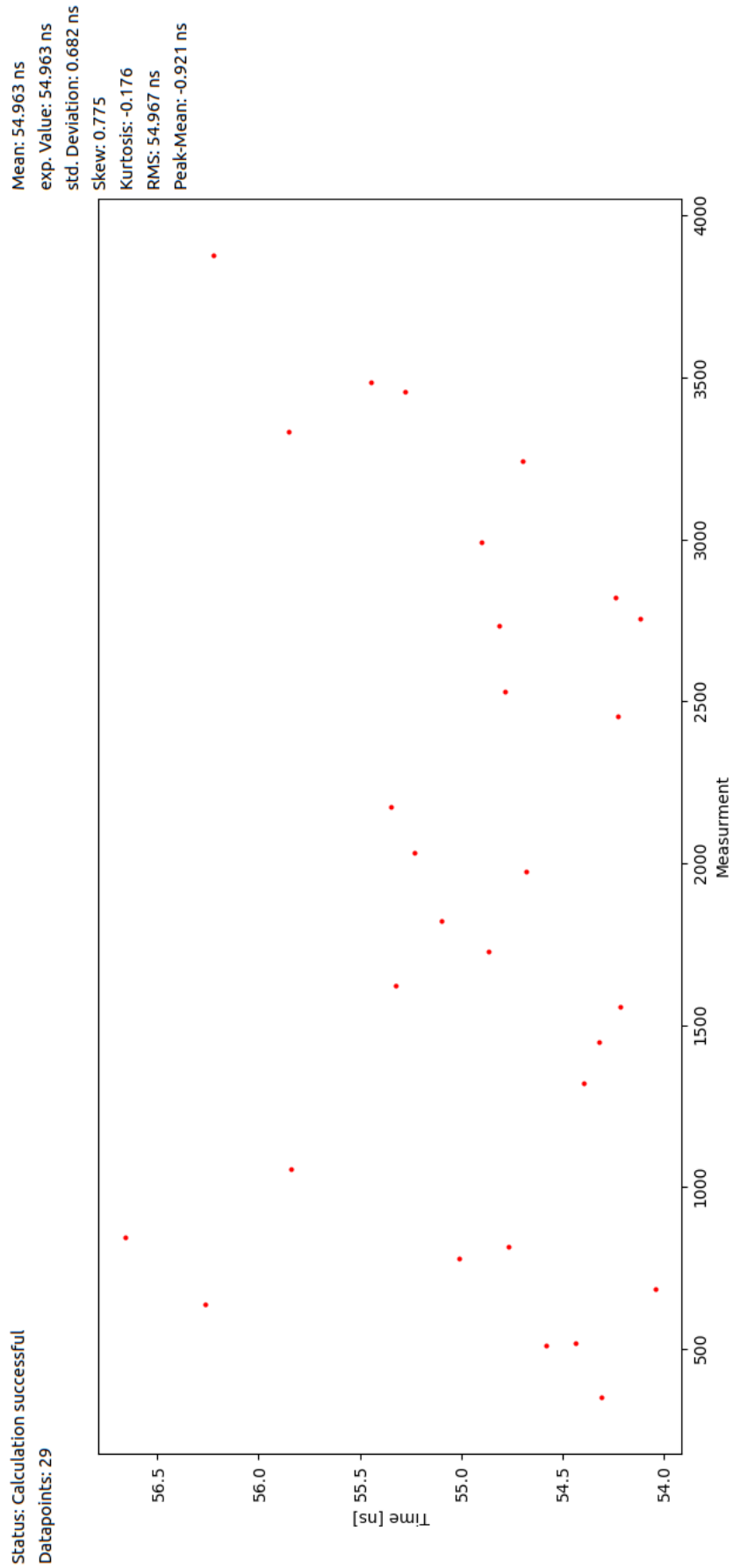


Figure 23: Absolute time walk SAP500, ND5

Mean: 84.884 ns
 exp. Value: 84.884 ns
 std. Deviation: 0.061 ns
 Skew: -0.066
 Kurtosis: -0.44
 RMS: 84.884 ns
 Peak-Mean: -0.013 ns

Status: Calculation successful
 Datapoints: 3803

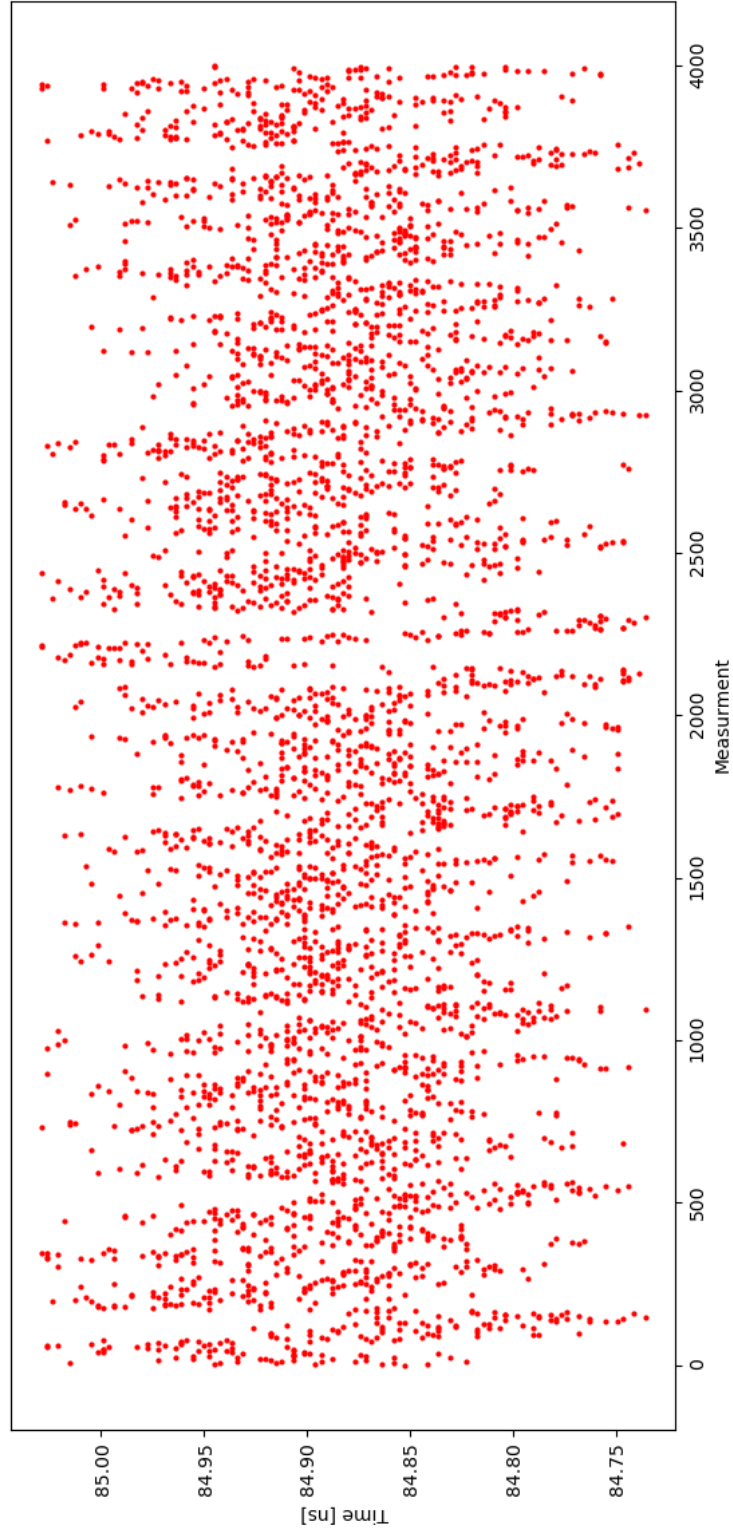


Figure 24: Compensated time walk SAP500, ND0

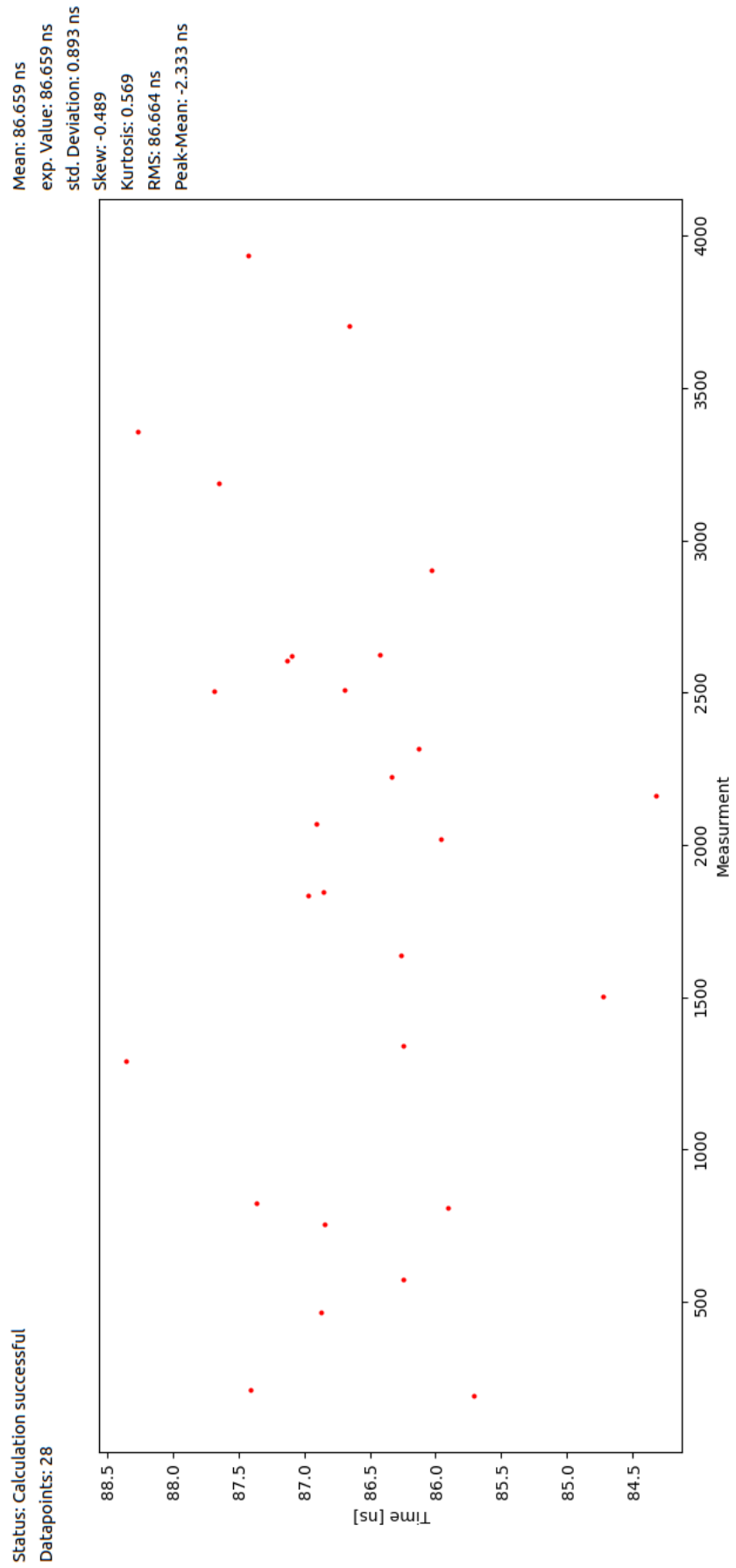


Figure 25: Compensated time walk SAP500, ND5

Mean: 51.098 ns
 exp. Value: 51.098 ns
 std. Deviation: 0.036 ns
 Skew: -0.01

Kurtosis: -0.582
 RMS: 51.098 ns
 Peak-Mean: -0.002 ns

Status: Calculation successful
 Datapoints: 3838

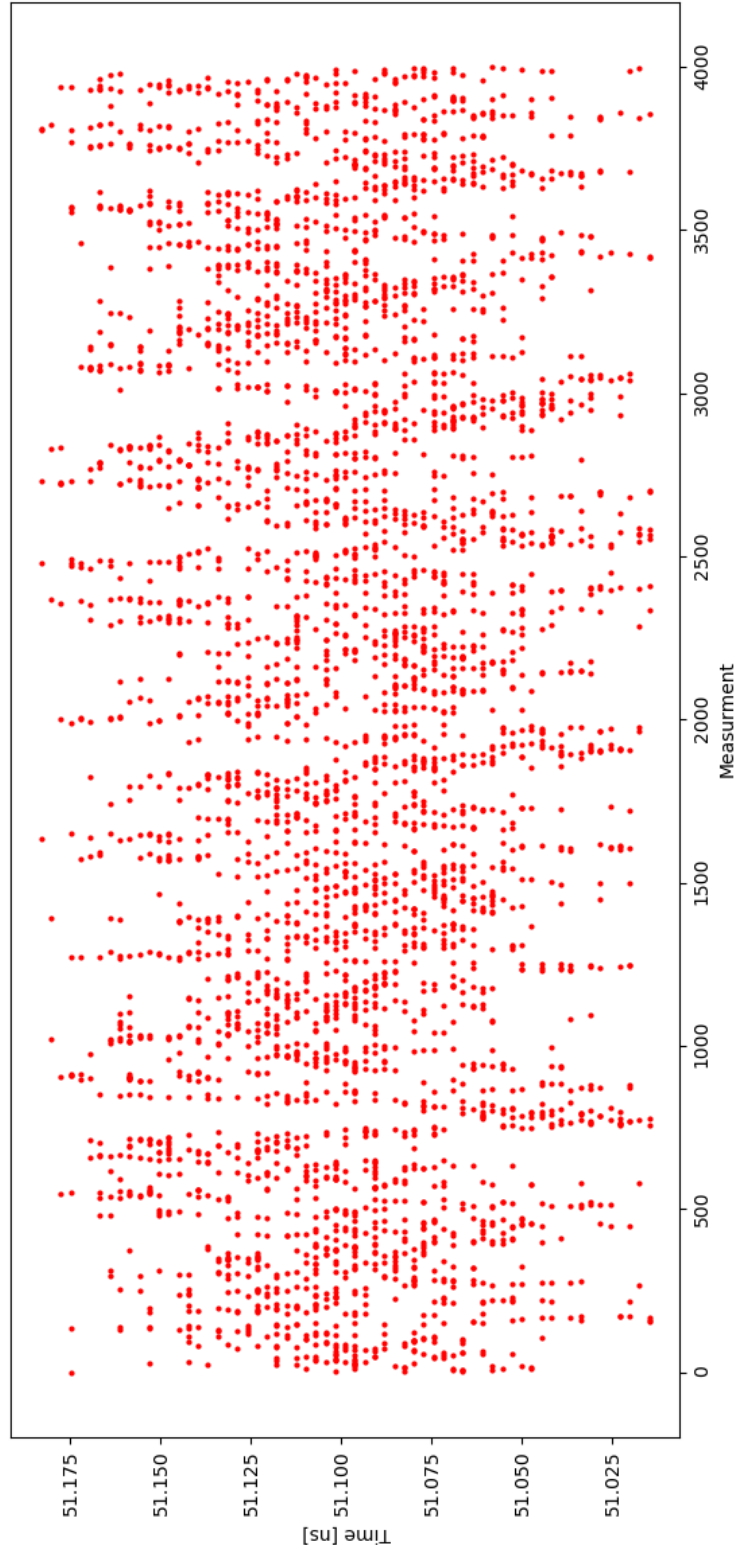


Figure 26: Relative time walk SAP500, ND0

Mean: 51.316 ns
 exp. Value: 51.316 ns
 std. Deviation: 0.1 ns
 Skew: 0.114
 Kurtosis: -1.217
 RMS: 51.317 ns
 Peak-Mean: -0.08 ns

Status: Calculation successful
 Datapoints: 1170

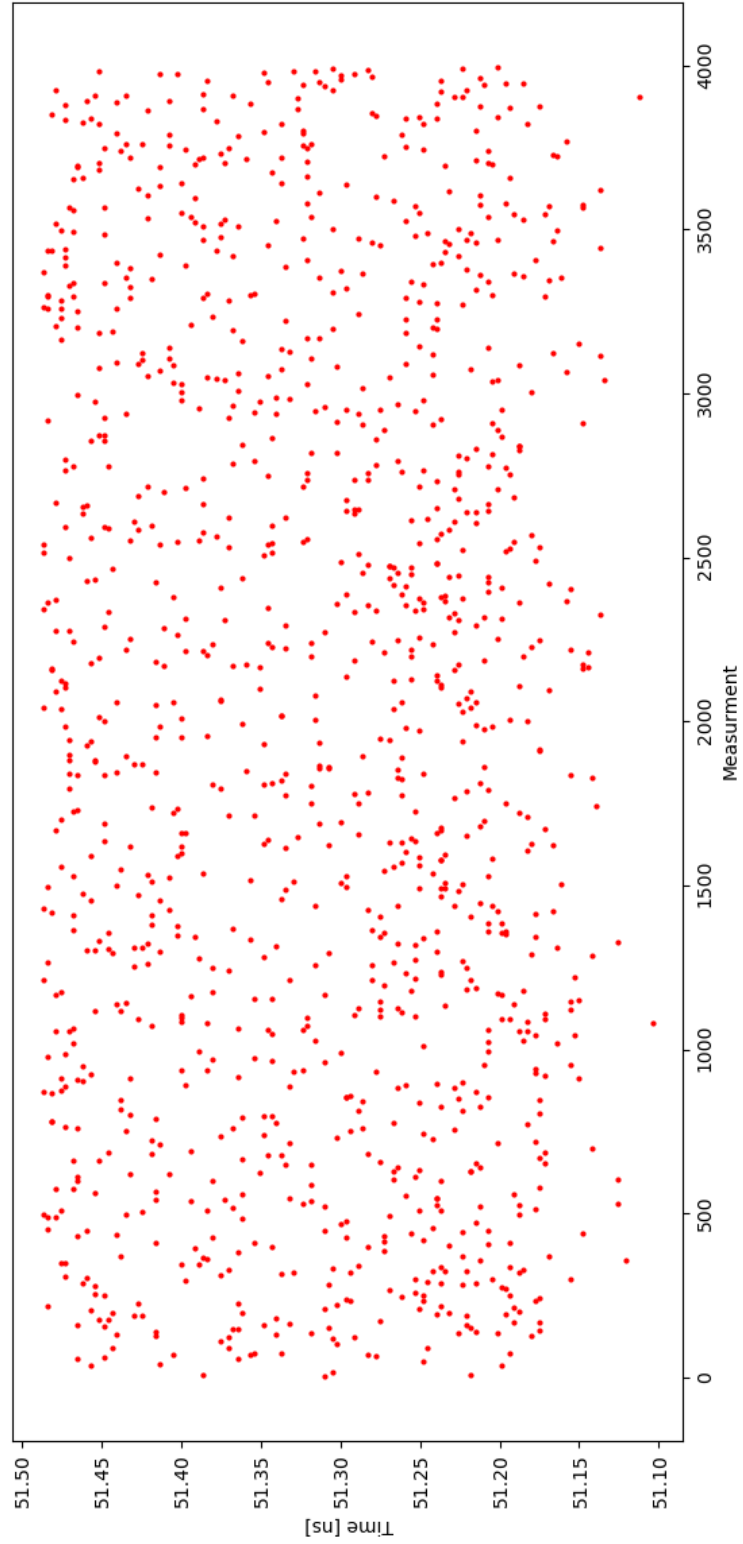


Figure 27: Relative time walk SAP500, ND4